Measuring Everything You've Ever Wanted to Know About an Ultrashort Light Pulse

Rick Trebino, Pamela Bowlan, Pablo Gabolde, Xun Gu, Selcuk Akturk, and Mark Kimmel

Georgia Institute of Technology, School of Physics, Atlanta, GA 30332 USA
rick.trebino@physics.gatech.edu

Abstract

We review the problem of measuring an ultrashort laser pulse and then describe several experimentally simple, accurate, and very reliable methods for measuring both very simple laser pulses and very complex ultrashort light pulses. Each of these methods comprises only a few easily aligned components, and they allow the measurement of a wide range of pulses, including those with time-bandwidth products greater than 1000 and those with energies of only a few hundred photons. Finally, two recently introduced very simple methods allow the measurement of the *complete spatio-temporal intensity and phase* of even complex pulses on a single shot or at a tight focus. In short, pulse-measurement technology is now so powerful and easy to use that it is time to use these methods and to focus on their applications.

Measuring Everything You've Ever Wanted to Know About an Ultrashort Light Pulse

Rick Trebino, Pamela Bowlan, Pablo Gabolde, Xun Gu, Selcuk Akturk, and Mark Kimmel

Georgia Institute of Technology, School of Physics, Atlanta, GA 30332 USA
rick.trebino@physics.gatech.edu

A Short Pre-History of Ultrashort-Laser-Pulse Measurement

In the 1960s, researchers began generating laser pulses shorter than could be measured using electronic detectors, and the field of ultrashort-laser-pulse measurement was born. How to measure humankind's shortest events? The goal was (and still is) to measure the pulse electric field vs. time, that is, its intensity, $I(t)$, and phase, $\phi(t)$:

$$E(t) = \mathrm{Re}\left\{\sqrt{I(t)}\exp\left[i(\omega_0 t - \phi(t))\right]\right\}$$

or, equivalently, in the frequency domain, the pulse spectrum, $S(\omega)$, and spectral phase, $\varphi(\omega)$:

$$\tilde{E}(\omega) = \sqrt{S(\omega)}\exp\left[-i\varphi(\omega)\right]$$

omitting the negative-frequency component of the pulse.

In principle, a shorter event is necessary to make the measurement. But clearly no such event was available. Researchers quickly realized that the shortest event available was the event itself. Thus autocorrelation[1] was born. Autocorrelation involved splitting the pulse into two, spatially overlapping the two pulses in some instantaneously responding nonlinear-optical medium, such as a second-harmonic-generation (SHG) crystal (See Fig. 1), and variably delaying one pulse with respect to the other. A SHG crystal produces light at twice the frequency of the input light with a field that is the product of the two input-pulse fields—and so only generates second harmonic when the pulses overlap in time, thus yielding a rough measure of the pulse length.

Measuring the SH pulse energy vs. delay yielded the autocorrelation of the pulse, which is given by:

$$A(\tau) = \int_{-\infty}^{\infty} I(t)\,I(t-\tau)\,dt$$

where τ is the relative delay between the two pulses.

But using the event to measure *itself* wasn't quite good enough. It was only *as short as* the pulse. It wasn't *shorter*. As a result, autocorrelation yielded a blurry picture of the pulse intensity vs. time.
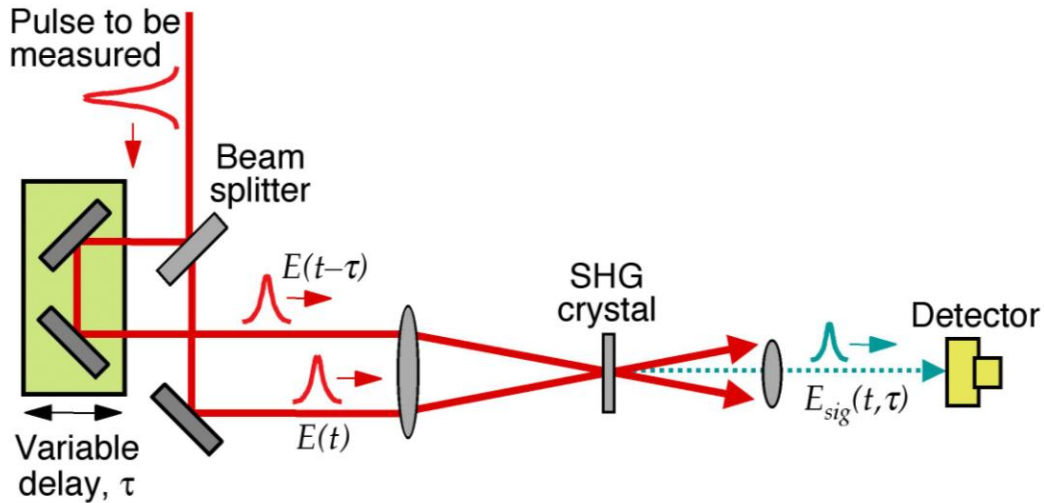
Fig. 1. Schematic of an autocorrelator, often called an intensity autocorrelator to distinguish it from its interferometric cousin, which uses collinear input beams.

It was necessary to assume a pulse shape in order to obtain a pulse length. Worse, the attempt to extract the pulse intensity from its autocorrelation is mathematically equivalent to the problem of retrieving the spectral phase when one has only the pulse spectrum. Obviously this is not possible, and, just as infinitely many possible spectral phases are consistent with a given spectrum, usually infinitely many pulse intensities vs. time correspond to a given autocorrelation trace. This notoriously ill-posed problem is called the *one-dimensional phase-retrieval problem*.[2-5] Finally, by design, autocorrelation yielded no information at all about $\phi(t)$.
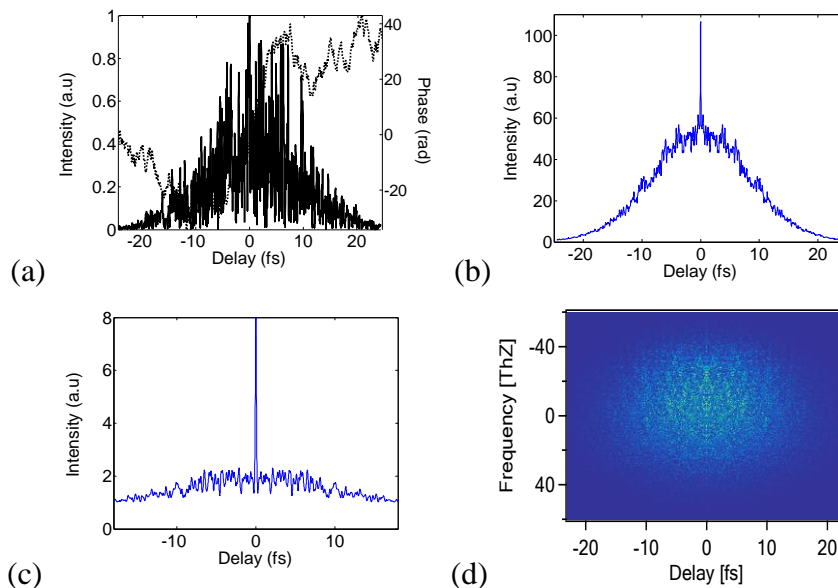

Fig. 2. (a) Complex pulse, (b) Its intensity autocorrelation, (c) Its interferometric autocorrelation, (d) Its SHG FROG trace. Note the high-visibility, extreme complexity of the SHG FROG trace, compared with the nearly washed-out structure of the autocorrelations.

Nowhere does the lack of power of the autocorrelation to reveal structure in a pulse reveal itself more than in the measurement of complicated pulses. In fact, for complex pulses, it can be shown that, as the intensity increases in complexity, the autocorrelation actually becomes *simpler* and approaches a simple shape of a narrow spike on a pedestal, *independent of the intensity structure*.[6]

In the 1980's, an interferometric version of autocorrelation[7-10] yielded some phase information, but no pulse-retrieval algorithm has ever been found for it, and it continued to require an assumed shape for the pulse intensity and phase. Attempts have been made to include additional information, such as the spectrum, but only very very simple pulses have been measured in this manner. As can be seen in Fig. 2, interferometric autocorrelation is also clearly a badly ill-posed problem—for a given measured trace, there are many (often infinitely many) possible pulses,[11] and no one knows how to find them. Even if one could determine all the possible pulses corresponding to a given trace, it is not possible to determine which one is the correct one.

It became customary to measure the pulse (intensity or interferometric) autocorrelation and spectrum and, taking the product of the two widths, obtain a rough estimate of the pulse time-bandwidth product (TBP). The details of the pulse could not be determined.

FROG and XFROG

In 1991 Kane and Trebino introduced Frequency-Resolved Optical Gating (FROG), a simple *spectrally resolved autocorrelation*, which involved simply moving the spectrometer from beside the autocorrelator to behind it (see Fig. 3).[12-14]

FROG involves time-gating the pulse with itself, as in autocorrelation, but now measuring the *spectrum* vs. the delay between the two pulses. Occasionally, a well-characterized reference pulse is available (usually measured using FROG), and Cross-correlation FROG (XFROG) takes advantage of this, gating the unknown pulse with this reference pulse. The general expression for both FROG and XFROG traces is:

$$I_{XFROG}(\omega, \tau) = \left| \int_{-\infty}^{\infty} E_{sig}(t, \tau) \exp(-i\omega t) dt \right|^2 ,$$

where the signal field, $E_{sig}(t, \tau)$, is a function of time and delay, usually of the form $E_{sig}(t, \tau) = E(t) E_{gate}(t - \tau)$. In FROG, the gate function, $E_{gate}(t)$, is a function of the unknown input pulse, $E(t)$, that we are trying to measure. When using SHG as the nonlinear-optical process, $E_{gate}(t) = E(t)$, and when using polarization-gating (PG), $E_{gate}(t) = |E(t)|^2$. In XFROG, $E_{gate}(t)$ can be any known function (i.e., pulse) acting as the reference pulse. In general, $E_{sig}(t, \tau)$ can be any function of time and delay that contains enough information to determine the pulse.

The FROG and XFROG traces are spectrograms of the pulse (although the FROG trace might more scientifically be called the "auto-spectrogram" of the pulse) and, as a result, are generally very intuitive displays of the pulse.

To see why the FROG problem is much better behaved than autocorrelation, let $E_{sig}(t, \tau)$ be the one-dimensional Fourier transform with respect to Ω of some new signal field, $\hat{E}_{sig}(t, \Omega)$. It is easy to show (just do the Ω integration to obtain the previous equation) that:

$$I_{FROG}(\omega, \tau) = \left| \int\int \hat{E}_{sig}(t, \Omega) \exp(-i\omega t - i\Omega\tau) \, dt \, d\Omega \right|^2$$
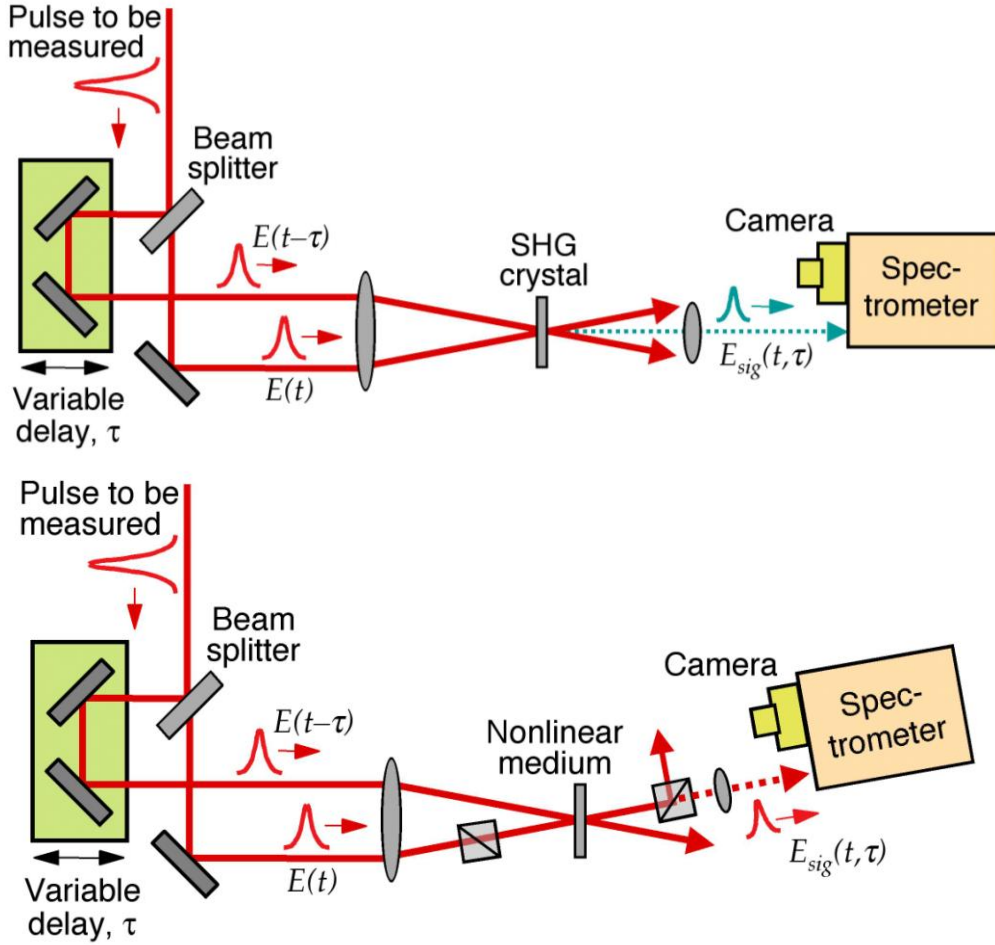
Fig. 3. Schematic of a FROG (frequency-resolved autocorrelation) apparatus. A pulse is split into two, and one pulse gates the other in a nonlinear-optical medium (above: a second-harmonic-generation crystal; below: polarization-gating in any medium). The second harmonic pulse (or polarizer leakage) spectrum is then measured vs. delay. XFROG involves an independent, previously measured gate pulse.

and, to determine the pulse field, $E(t)$, that it is sufficient to find $\hat{E}_{sig}(t,\Omega)$. Thus the FROG trace is the mag-squared two-dimensional Fourier transform of $\hat{E}_{sig}(t,\Omega)$. This is the *two-dimensional* relative of the one-dimensional phase-retrieval problem. And it has been shown that two-dimensional phase-retrieval problem, in strong contrast to the one-dimensional phase retrieval problem, is essentially well-posed (has only trivial ambiguities),[3] and simple, reliable iterative algorithms exist for finding the desired two-dimensional field,[3] $\hat{E}_{sig}(t,\Omega)$, and hence $E(t)$. A few so-called "trivial ambiguities" exist (see Table 1), but, fortunately, they are of little interest in most pulse-measurement problems. Also, the direction-of-time ambiguity is only present in SHG FROG (and not in XFROG or other versions of FROG), but this one-bit ambiguity is easily removed by simply adding a piece of glass in the beam and making a second trace, which is consistent with only one of the directions of time. Also, a few ambiguities exist for well-separated pulses in time and modes in frequency (such pulses are better measured using a properly designed XFROG, which does not have these ambiguities, but if one insists on using FROG, use of an etalon as the beam-splitter removes them and also the direction-of-time ambiguity if present[2, 15]). In any case, for all other pulses, FROG works extremely well.

Occasionally, a new possible ambiguity is reported,[16] but so far, all such reports have been found to be erroneous.[17]

Table 1. "Trivial ambiguities" in phase retrieval, that is, functions with the same Fourier-transform magnitude as $E(t)$. These ambiguities affect phase-retrieval problems in all dimensions, that is, whether it's a one-dimensional parameter or a multi-dimensional quantity. But they are not generally important in most fields, including ultrafast optics.

Function	Type of ambiguity
$E(t)$ $\exp(i\phi_0\Box)$	Absolute-phase shift
$E(t-t_0)$	Translation
$E^*(-t)$	Time-reversal

To retrieve pulses using FROG, we use modified phase-retrieval routines, which have proved very robust and fast, usually converging in < 0.1 second,[2] unless the pulse is very complex. Indeed, FROG has become an effective and versatile way to measure ultrashort laser pulses, whether a 20 fs UV pulse or an oddly shaped IR pulse from a free-electron laser.[2] And FROG now routinely measures the intensity and phase of few fs pulses, and variations on it are now measuring attosecond pulses.[18][19] No other method has approached FROG's success and versatility in measuring such a range of pulses.

As is often the case with new ideas, there are many misconceptions about FROG in the literature. For example, the simple trick of using an etalon as the beam-splitter in a FROG to remove the well-separated-pulse ambiguities[2, 15] is not well known, and, as a result, very complex methods have been introduced to remove these ambiguities. Unfortunately, complex methods are as likely to introduce a distortion as to measure it, and so such methods should only be used with extreme care. On the other hand, simply replacing the FROG beam-splitter with an etalon adds no complexity and works very well.

Also, because FROG involves an iterative pulse retrieval algorithm (an unusual feature of pulse-measurement techniques), many erroneously believe it to be "ill-posed," because some well-known iterative inverse problems are ill-posed (have ambiguities).[20] The most infamous ill-posed problem is arguably the inverse-heat-flow problem—determining the initial temperature distribution from a final, usually uniform, one—and is well known to be impossible, as many initial distributions are consistent or nearly consistent with the final one. A related class of less problematic, but nonetheless unpleasant, problems are "ill-conditioned" problems, which have approximate ambiguities (very similar experimental traces for very different pulses). Because *all* self-referenced pulse-measurement techniques fail to measure the absolute phase and the pulse arrival time, all are technically ill-posed in the strict sense. But if we recognize that these trivial ambiguities are not generally of interest (and other methods exist to measure them if one cares), then we can call characterize the "well-posedness" of a technique by how few such trivial ambiguities it has. We can begin by asking: can the technique measure the pulse *shape*, which is not affected by the trivial ambiguities, and which is what one generally cares about?

It turns out that FROG is actually the best-posed self-referenced pulse-measurement technique currently available. Aside from the above-mentioned trivial ambiguities, which all other self-referenced pulse-measurement techniques share, FROG uniquely determines the pulse intensity and phase for even very complex pulses. Intensity autocorrelation and interferometric autocorrelation, on the other hand, not only do not determine the pulse at all (they have no inversion algorithm at all), but such traces actually become simpler rather than more complex as the pulse increases in complexity, losing much information about the pulse—precisely the issue in the inverse heat-flow problem. Other self-referenced methods cannot measure complex pulses (TBPs no more than three or four have been measured by most), rendering them severely ill-

posed, as well, since all complex pulses have similar measured traces in these methods. In most other methods, complex pulses have similar traces to those of simple pulses, and one must assume that one has a simple pulse for them to yield an answer. FROG, on the other hand, has never been shown to have an ambiguity beyond those mentioned above. And variations on FROG, such as XFROG, can be used to avoid the few trivial ambiguities that are known.

Finally, it does not appear to be well appreciated that FROG has the convenient feature that it yields feedback confirming the measurement. Because the measured FROG trace massively over-determines the pulse, when the measured trace agrees with the retrieved trace, the measurement is very likely to have been performed correctly. If not, then the device could have been misaligned, or the input pulse may have had one or more of many spatio-temporal distortions, and the measurement should not be trusted. Because ultrashort pulse measurement can be very difficult, this feedback is important. No other technique offers this assurance.

What Next?

Now that we have achieved the ability to measure such ephemeral events reliably, it is important to transcend the measurement of mere ultrashort *laser* pulses, whose intensity and phase are well-behaved in space, time, and frequency, and which have fairly high intensity. It is important to be able to measure ultrashort *light* pulses, whose intensity and phase are *not* well-behaved in space, time, and frequency, and which often are not very intense. It is important to be able to measure such pulses as ultrabroadband continuum light pulses emerging from micro-structure optical fiber and weak luminescence from molecules important in biology and human physiology — light pulses whose measurement will lead to new technologies or teach us important things about life, not just how well our laser is aligned. And it is important to do so with a simple device, not one so complex that it could easily introduce the same distortions it hopes to measure. In short, the goal is, not a complex device that can only measure simple pulses, but a simple device that can measure complex pulses.

We have recently made significant progress in all of these areas. It is now possible to measure ultrashort light pulses whose time-bandwidth product exceeds 1000,[3] pulses with as little as a few hundred photons (and simultaneously with poor spatial coherence and random absolute phase),[4] and pulses with spatio-temporal distortions like spatial chirp and pulse-front tilt.[5,6] It is also possible to measure very complex pulses in a train in which each is different.[3] And no less than two different techniques allow us to measure the *complete spatio-temporal field* of pulses. One technique can do so on a single shot,[21, 22] but not at a focus. The other can measure pulses at a focus,[23-25] but not on a single shot. In fact, all of these techniques are quite easy to perform, involving only a few easily aligned elements. And they are easily aligned, reliable, and quite general.

Of course, measuring ultrashort *laser* pulses remains easier than measuring more complex ultrashort *light* pulses, but, recently, measuring ultrashort laser pulses became *extremely* easy. We introduced a new variation of FROG, called GRENOUILLE,[26-28] which has no sensitive alignment knobs, only a few elements, and a cost, weight, and size considerably less than previously available devices (including now obsolete autocorrelators). GRENOUILLE yields traces identical to those in FROG, and hence yields the full pulse intensity and phase for arbitrary pulses using the same commercially available computer algorithm. It can do so for as little as a single laser pulse, and, because it uses a *thick* nonlinear crystal (unlike other pulse-measurement methods, which require extremely thin crystals, yielding very few signal photons), it is also very sensitive — more sensitive than autocorrelators. GRENOUILLE also measures the first-order spatio-temporal distortions, spatial chirp and pulse-front tilt,[29, 30] without the need for modifications in its apparatus. GRENOUILLE can also be arranged so that it measures the beam spatial profile, as well, so that it can accurately be said that GRENOUILLE measures essentially every quantity of interest about an ultrashort laser pulse! GRENOUILLE is already

in use in several hundred labs all over the world, and it is rapidly becoming the standard for ultrashort laser pulse monitoring.

Measuring Extremely Complex Pulses Using FROG and XFROG

Unlike intensity autocorrelation and interferometric autocorrelation, whose traces actually become simpler as the pulse becomes more complex, FROG traces become significantly more complex as the pulse becomes more complex. This implies that the information necessary to determine the complex pulse continues to reside in the FROG trace even as the pulse becomes very complex. Indeed, FROG has recently been shown to be capable of measuring exceedingly complex pulses (see Fig. 4).[31] In this study of pulses with TBPs as large as 100, XFROG proved successful at retrieving all pulses on the first initial guess, despite the presence of noise. PG and SHG FROG were able to retrieve approximately 95% and 85%, respectively, of the extremely complex pulses in the study. And if the algorithm fails to converge for such complex pulses, it is clear from the discrepancy between the measured and retrieved traces, so one simply tries additional initial guesses until convergence occurs.
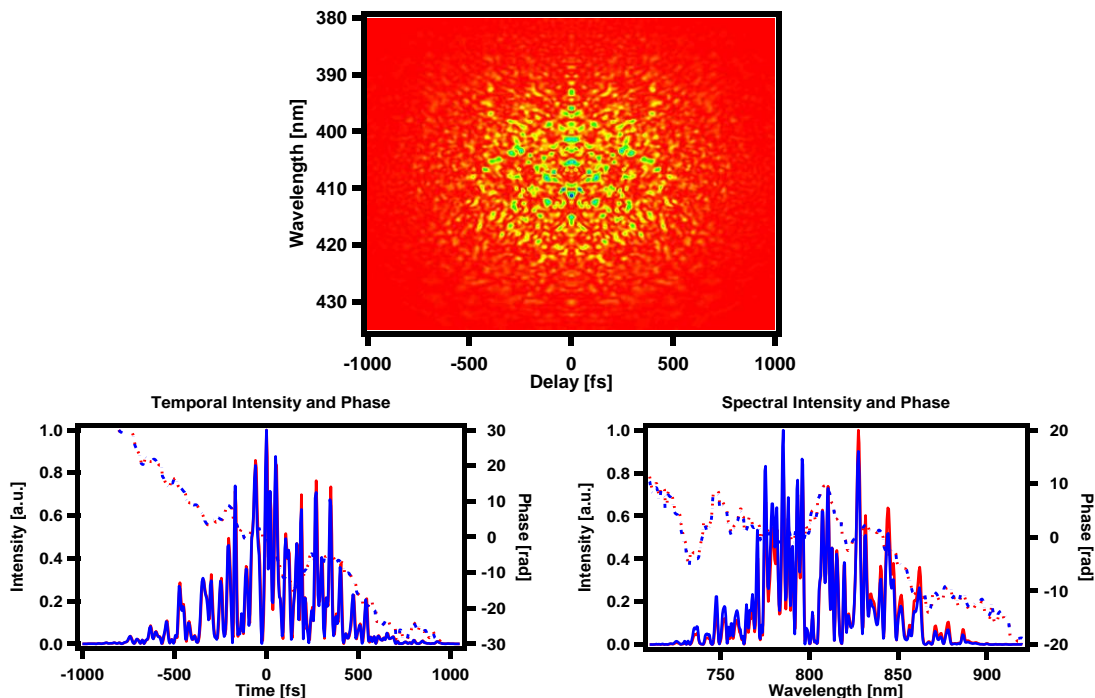

Fig. 4. SHG FROG for an extremely complex pulse. Top: SHG FROG trace of a pulse with a time-bandwidth product of approximately 100. Bottom, the actual (red) and retrieved (blue) pulses.

But how does FROG perform for complex pulses in practice? Arguably, the most complex ultrashort pulse ever generated is ultrabroadband supercontinuum, which can now be generated easily in recently developed microstructure and tapered optical fiber, using only nJ input pulses from a Ti:Sapphire oscillator.[32] Many applications of the supercontinuum require good knowledge of the light, especially its phase. In an effort to characterize the intensity and phase of this extremely complicated pulse, XFROG is so far the only technique that has been able to successfully measure this pulse.[33] Not only does XFROG deliver an experimental trace that allows the retrieval of the intensity and phase of the pulse in both the time and frequency domains (and even more, as will be clear below), but the XFROG trace itself, which is a

spectrogram of the pulse, also proves to be a very intuitive tool for the study of the generation and propagation of the supercontinuum and so is also used by theorists to plot continua. Many individual processes important in supercontinuum generation, such as soliton generation and fission, can be much more easily identified and studied by observing the XFROG trace than by considering the temporal or spectral intensity and phase.

An XFROG apparatus is shown in Fig. 5. The main challenge in attempting to use XFROG (or any other potential method) to measure the supercontinuum is obtaining sufficient bandwidth in the SFG crystal: the entire spectrum of the continuum must undergo sum-frequency generation (SFG) with the reference pulse (achieve "phase-matching") for the measurement to be correct. This typically requires using an extremely thin crystal, in this case a sub-five-micron crystal, which is not practical, and which would generate so few SFG photons that the measurement would not be possible were it to be used. Instead we angle-dither a considerably thicker (1 mm) crystal[33] to solve this problem. Because the crystal angle determines the frequencies that are phase-matched in the SFG process, varying this angle in the course of the measurement allows us to obtain as broad a range of phase-matched frequencies as desired. It is only necessary to phase-match the entire pulse spectrum over the course of the measurement and not on each and every pulse in the measurement, as previously believed.
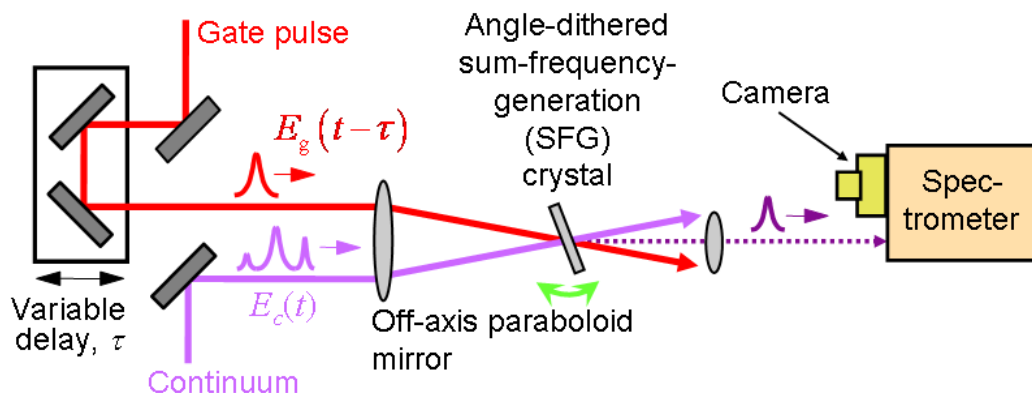

Fig. 5. Schematic diagram of our multi-shot XFROG measurement apparatus.

We performed the first XFROG measurement of the microstructure-fiber supercontinuum on pulses generated in a 16-cm-long microstructure fiber with an effective core diameter of ~ 1.7 microns. In the measurement, we performed SFG between the supercontinuum and the 800 nm Ti:Sapphire pump pulse as the nonlinear gating process. In order to phase-match all the wavelengths in the supercontinuum, the nonlinear crystal (BBO) was rapidly dithered during the measurement with a range of angles corresponding to the entire supercontinuum bandwidth. The experimental trace was parabolic in shape, in agreement with the known group-velocity dispersion of the fiber (Fig. 6). The supercontinuum pulses had a time-bandwidth product of $\sim$ 4000, by far the most complicated pulses ever characterized. Despite the general agreement between the measured and retrieved traces, the results from the intensity-and-phase retrieval were somewhat unexpected: the retrieved trace contained an array of fine structure not present in the measured trace, and the retrieved spectrum also contained ~ 1 nm-scale fine structure, contrary to the smooth spectrum previous measurements using simple spectrometers had shown. However, we then performed difficult *single-shot* spectral measurements (using a spectrometer), which confirmed our findings, that is, the ~ 1 nm-scale fine features do exist in the supercontinuum spectrum, but only on a single-shot basis, as wild shot-to-shot fluctuations wash them out completely in multi-shot measurements in spectrometers. These fine spectral features agree with theoretical calculations very well.[34-37]

XFROG was able to recover the unstable fine spectral features due to the intrinsic information redundancy of FROG traces. Indeed, all FROG traces are two-dimensional temporal-spectral representations of a complex field, and the two axes are two sides of one coin. The same information

9

is present in both axes. In this case, the unstable fine spectral features also correspond to slow temporal modulations. Although the experimental XFROG trace that we measured lacked the fine spectral features because our measurement was made on a multi-shot basis, the long temporal features in the traces, however, were sufficient to assist the retrieval algorithm to find a result with fine spectral features. This is another advantage of FROG: lost frequency resolution is recoverable from the FROG measurement via redundant temporal information.
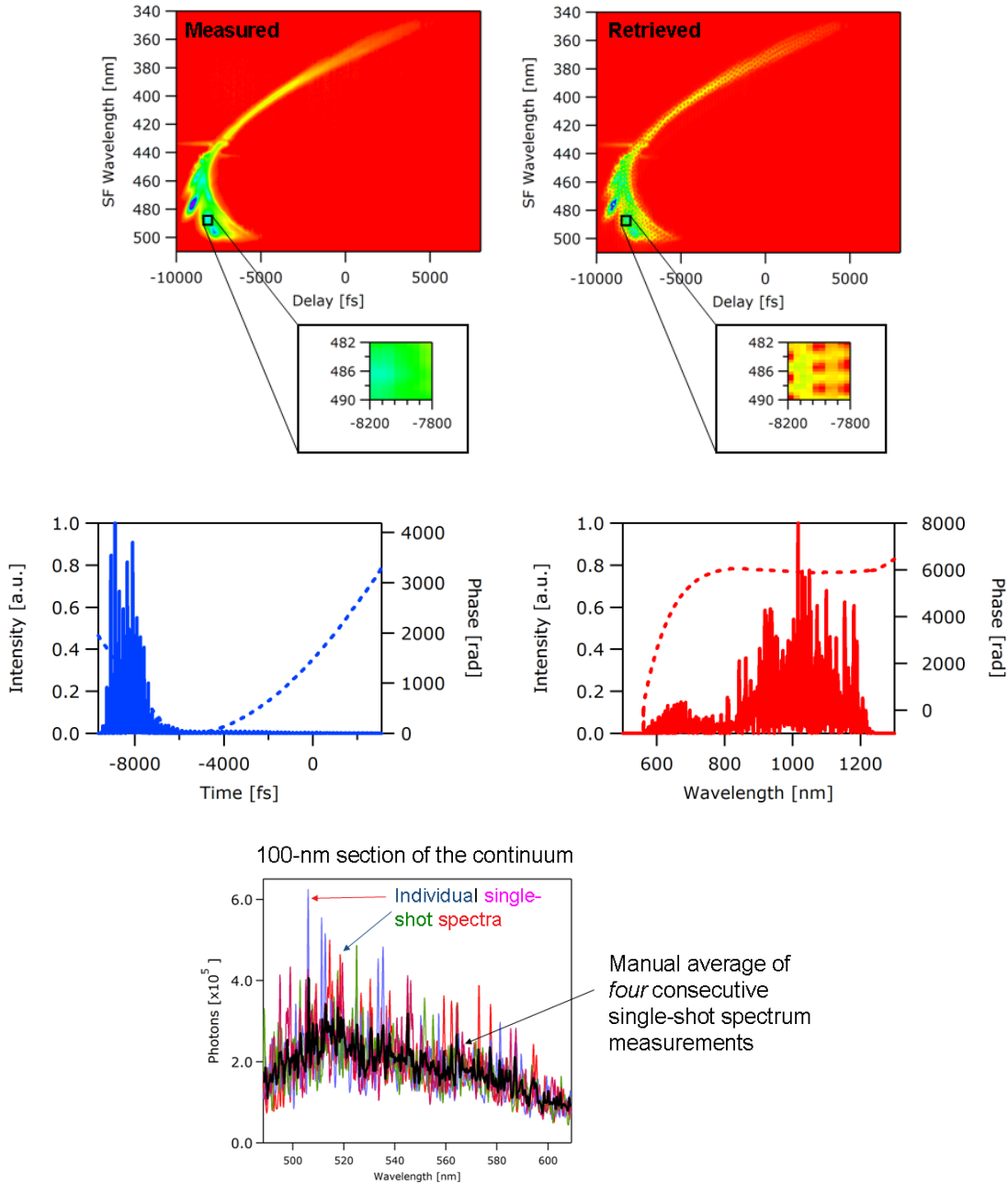
Fig. 6. XFROG measurement of microstructure-fiber continuum with an 800 nm, 30 fs pre-characterized reference pulse. Upper left: measured trace; Upper right: retrieved trace. The insets are higher-resolution sections in the traces.; Middle left: retrieved temporal intensity (solid) and phase (dash); Middle right: retrieved spectral intensity

10

(solid) and phase (dash); Bottom: a 100-nm portion of the spectrum measured using a spectrometer on a single shot. The XFROG error was 0.012 for the 8192 × 8192 traces.

The newly revealed fine spectral structure and shot-to-shot-instability of the supercontinuum pulses presented profound and often undesirable implications to the application of this light. But these results have been instrumental in understanding the underlying spectral broadening mechanisms and in confirming recent advances in numerical simulations of supercontinuum generation in microstructure fiber. Simulations using the extended nonlinear Schrödinger equation (NLSE) model have matched experiments amazingly well. [34-37]   Although most microstructure-fiber supercontinuum experiments at the time used 10-100 cm of fiber, simulations have revealed that most of the spectral broadening occurs in the first few mm of fiber. Further propagation, which only slowly broadens the spectrum through less significant nonlinear processes, such as Raman self-frequency shift, yields only increasingly unstable and fine spectral structure due to the interference of multiple solitons in the continuum spectrum.

This observation suggested that use of a short (< 1 cm) length of microstructure fiber would still yield supercontinuum generation, and the resulting continuum will still be broad, but short, more stable, and with less fine spectral structure.   To test this hypothesis, we generated supercontinuum in an 8 mm-long microstructure fiber with 40 fs Ti:Sapphire oscillator pulses and performed similar XFROG measurements of it.[38]

We see from Fig. 7 that the retrieved trace is in good agreement with the measured one, reproducing all the major features. The additional structure that appears in the retrieved trace can be attributed to some remaining shot-to-shot instability of spectral fine structure in the
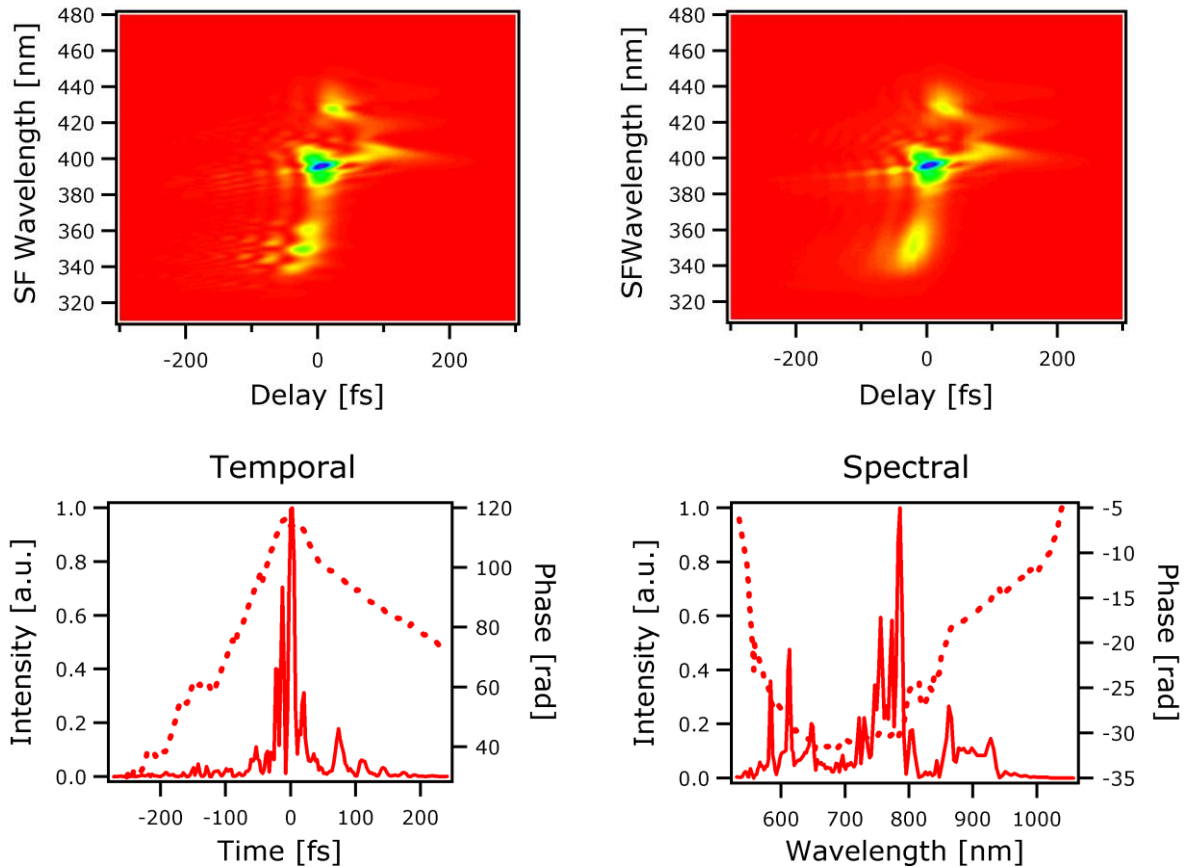

Fig. 7. XFROG measurement and retrieved pulse for the 8 mm-long microstructure-fiber continuum with an 800 nm 40 fs pre-characterized reference pulse: (a) measured trace,

(b) retrieved trace, (c) retrieved temporal intensity (solid) and phase (dashed), (d) retrieved spectral intensity (solid) and phase (dashed).

continuum spectrum as discussed in detail above. The retrieved continuum intensity and phase vs. time and frequency are shown in the bottom panels of Fig. 7. The most obvious feature in this figure is that the continuum from the 8 mm-long fiber is significantly shorter than the picosecond continuum generated in the 16 cm-long fiber and, indeed, consists of series of sub-pulses that are shorter than the input 40 fs pulse. At the same time, the short-fiber continuum has less complex temporal and spectral features than the continuum pulses measured from longer fibers previously. The spectral phase of the short fiber continuum varies only in the range of 25 rad, which is relatively flat compared with the spectral phase of the long-fiber continuum, which is dominated by cubic phase spanning over 1000π rad.

In view of the complexity of the continuum, we made an independent measurement of the continuum spectrum using a spectrometer and averaged over $\sim 10^7$ pulses. We found excellent agreement between the retrieved spectrum and that independently measured using the spectrometer (not shown). Slight discrepancies were also due to fluctuations in the spectrum from shot to shot in the continuum, which smear out the spectrometer-measured, but not the FROG-measured, spectrum.

In conclusion, XFROG has been the only method to successfully measure the intensity and phase of the microstructure-fiber continuum, arguably the world's most complicated pulse (in our case, a time bandwidth product ~ 4000 from a 16 cm fiber). These measurements have revealed unstable nm-scale features in the continuum spectrum. Measurements performed on the continuum generated from an 8 mm fiber show that a short fiber generates more stable and less complicated pulses.

Measuring Ultraweak Pulses

Whereas measuring continuum is challenging due to its extreme complexity and instability, the continuum from micro-structure fiber is nonetheless usually a relatively intense (nJ), spatially coherent beam. Unfortunately, this cannot be said of ultrashort fluorescence from scientifically interesting "non-fluorescent" bio-luminescent molecules. Most biologically important excitations decay rapidly and yield extremely weak luminescence, since the biological use must compete with fluorescence. Such pulses are also spatially incoherent, and they have random absolute phase. While their measurement would yield important insight into the dynamics of many biological processes,[39] their measurement proves even more challenging. Indeed, interferometric methods, such as spectral interferometry, which are well-known for their high sensitivity, prove inadequate for such measurements due to both the light's spatial incoherence and random absolute phase.

However, there is an XFROG technique capable of measuring trains of few-photon spatially incoherent light pulses with random absolute phase.[40] It involves spectrally resolving a time-gated pulse and measuring its spectrum as a function of delay to yield an XFROG trace or a spectrogram of the pulse. The nonlinearity used in this technique, however, is Optical Parametric Amplification (OPA) or Difference Frequency Generation (DFG), which involves not only time-gating the pulse to be measured, but also *amplifying* it in the process. The weak pulses are amplified by up to $\sim 10^5$ by an intense, bluer, shorter, synchronized gate pulse and then spectrally resolved to generate an OPA XFROG trace. We then use a modified FROG retrieval algorithm to retrieve the intensity and phase of the ultraweak pulse measured from the OPA XFROG trace.

In addition to the above complexities, ultrafast fluorescence is also broadband. We use a noncollinear OPA (NOPA) geometry in order to phase-match the broad bandwidth while

scanning the delay and generating the OPA XFROG trace. Group Velocity Mismatch (GVM) becomes an important issue in time-gating such broadband pulses with the much shorter gate pulse. But GVM can be minimized in the OPA XFROG measurement by using the NOPA geometry as well. A suitable crossing angle can be chosen so that the GVM is minimized while simultaneously maximizing the phase-matched bandwidth. This allows the use of thicker OPA crystals to improve the gain.

In both OPA and DFG, a strong bluer "pump" pulse is coincident in time in a nonlinear-optical crystal with another pulse (which, in the OPA literature, is usually called the "signal" pulse, but we will avoid this terminology as it conflicts with our use of the term "signal," and call it "unknown pulse" instead). If the pump pulse is strong, it exponentially amplifies both the unknown pulse (OPA) and also noise photons at the same frequency (usually referred to as the optical parametric generation, or OPG, process), and simultaneously generating difference-frequency (DFG, often called the "idler") photons. Either the OPA or the DFG pulse can be spectrally resolved to generate an XFROG trace.

From the coupled-wave OPA equations, the electric field of the OPA XFROG signal from the crystal has the form:

$$E_{sig}^{OPA}(t,\tau) = E(t) f_{gate}^{OPA}(t-\tau),$$

where, as before, E(t) is the unknown input pulse and we have assumed that the pump pulse intensity remains unaffected by the process, which should be valid when the pulse to be measured is weak and we only need to amplify it enough to measure it. The OPA gate function is given by:

$$f_{gate}^{OPA}(t-\tau) = \cosh\left(g\left|E_{ref}(t-\tau)\right|z\right).$$

where the gain parameter, g, is given by the expression:

$$g = \frac{4\pi d_{eff}}{\sqrt{n_{OPA}\lambda_{OPA}}\sqrt{n_{DFG}\lambda_{DFG}}}$$

Thus the unknown pulse undergoes exponential gain during OPA. And very importantly, *the gating and gain processes do not alter the pulse phase*.

It must be pointed out that, in OPA XFROG, unlike other FROG methods, the input pulse is present as a background, even at large delays in the OPA XFROG trace. The equation and the corresponding XFROG algorithm take this into account while retrieving the intensity and phase of the pulse. For high gain, this background becomes negligible.

In the case of DFG XFROG, the idler is spectrally resolved to yield the DFG XFROG trace. Although it has been known that DFG can be used to measure fairly weak pulses,[27] the method has never been demonstrated for cases with gain. Including the effect of gain the DFG electric field is given by:

$$E_{sig}^{DFG}(t,\tau) = E(t) f_{gate}^{DFG}(t-\tau)^{*}.$$

The unknown input pulse here is the same as in the case of OPA. The gate function now has the form:

$$f_{gate}^{DFG}(t-\tau) = \exp\left(i\phi_{ref}(t-\tau)\right)\sinh\left(g\left|E_{ref}(t-\tau)\right|z\right),$$

where $\phi_{ref}(t-\tau)$ is the phase of the reference pulse. If the reference pulse is weak, the net gain is small and the above expression reduces to the form $f_{gate}^{DFG}(t-\tau) = E_{ref}(t-\tau)$.

The unknown pulse can thus be easily retrieved from the measured trace using the iterative XFROG algorithm, modified for the appropriate gate pulse. For high gains, the reference-gate pulse experiences gain-shortening in time, a desirable effect. GVM between the gate pulse (commonly referred to as the pump pulse for the OPA process) and the unknown pulse can distort measurement of phase by affecting the gain experienced by the unknown pulse. Thus the interaction length between the pump and unknown pulse during parametric amplification is limited by GVM. The larger the GVM, the shorter the interaction length will be. Therefore, in order to obtain gain over the entire bandwidth, it is necessary to choose a crystal whose length is of the order of, but less than, the interaction length.

It is also possible to eliminate GVM in OPA XFROG by crossing the pump and unknown pulse at a crossing angle, which can be calculated for specific wavelengths using a public domain computer program "GVM" within nonlinear optics software SNLO. The non-collinear geometry is particularly useful in working with broadband pulses, since it is possible to choose an optimal crossing angle that will minimize the GVM over the entire bandwidth range, while simultaneously allowing the entire bandwidth to be phase-matched.

A typical experimental set-up for OPA/DFG XFROG is shown in Fig. 8. In our experiments, an amplified 800 nm pulse was first characterized using a commercially available Swamp Optics GRENOUILLE. The pulse was then split into two. One pulse generated a white-light continuum (with poor spatial coherence) in a 2 mm thick sapphire plate, which was then spectrally filtered using a band-pass filter to yield a narrow spectrum. This pulse was attenuated using neutral density filters to act as the weak unknown pulse.
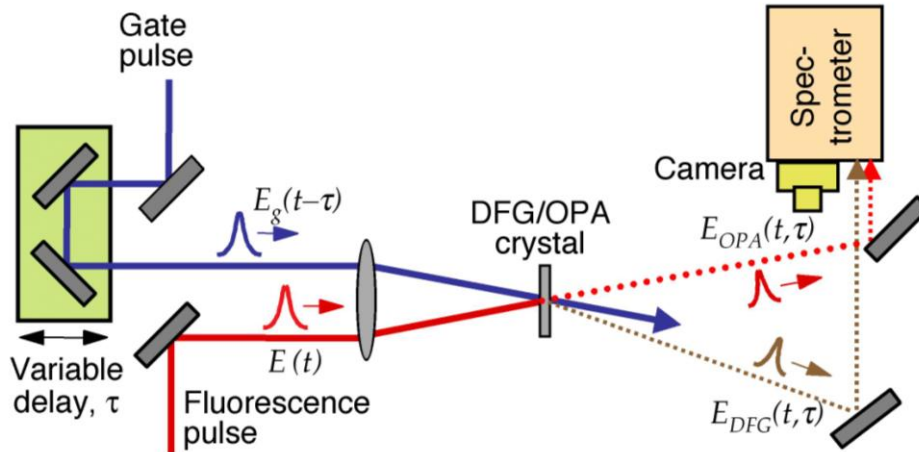

Fig. 8. Schematic of experimental apparatus for OPA or DFG XFROG.

The other pulse was frequency-doubled using a 1 mm thick Type I BBO crystal and passed through a variable delay line to act as the gate (pump) pulse for the OPA process. The two pulses were focused at a ~3° crossing angle using a 75 mm spherical mirror into a 1 mm BBO Type I crystal. The resulting OPA signal was spectrally resolved and imaged onto a CCD camera integrated over a few seconds.

In the first case, we attenuated the filtered white light continuum to 80 fJ and measured its OPA XFROG trace. The pulse in this case experienced an average gain of about $\cosh(5.75) \sim$ 150. Its intensity and phase retrieved using the OPA XFROG algorithm are shown in Fig. 9. A comparison of the intensity and phase of the same pulse, unattenuated at 80 pJ, is also shown. This was made using the less sensitive, but well established, technique of SFG XFROG. Both techniques yielded identical pulses and the independently measured spectrum of the filtered white light matched well with the OPA XFROG retrieved spectrum. This established OPA

XFROG as a pulse measurement technique that could measure pulses ~10^3 weaker than those measured by SFG XFROG.

Next we pushed the technique much harder by attenuating the filtered white light continuum down to 50 aJ and retrieved its intensity and phase using the OPA XFROG technique. Shown in Fig. 10 are the measured traces with their intensity and phase retrieved for an average gain of G ~ 10^5. The OPA signal was only about 5 times more intense than the background caused by OPG in the nonlinear crystal. This background is likely to be the lower limit on how weak the unknown pulse can be and still be measured accurately using the OPA XFROG technique. Despite this, OPA XFROG is the most sensitive ultrashort-pulse measurement technique, capable of measuring pulse trains with an average power of tens of fW, considerably better that interferometric techniques such as spectral interferometry, which have been demonstrated in measuring high-repetition-rate trains of pulses with zJ (10^{-21} J) of pulse energy, but with average powers of hundreds of fW.

Measured OPA XFROG Trace

Retrieved OPA XFROG Trace

Temporal Intensity and Phase
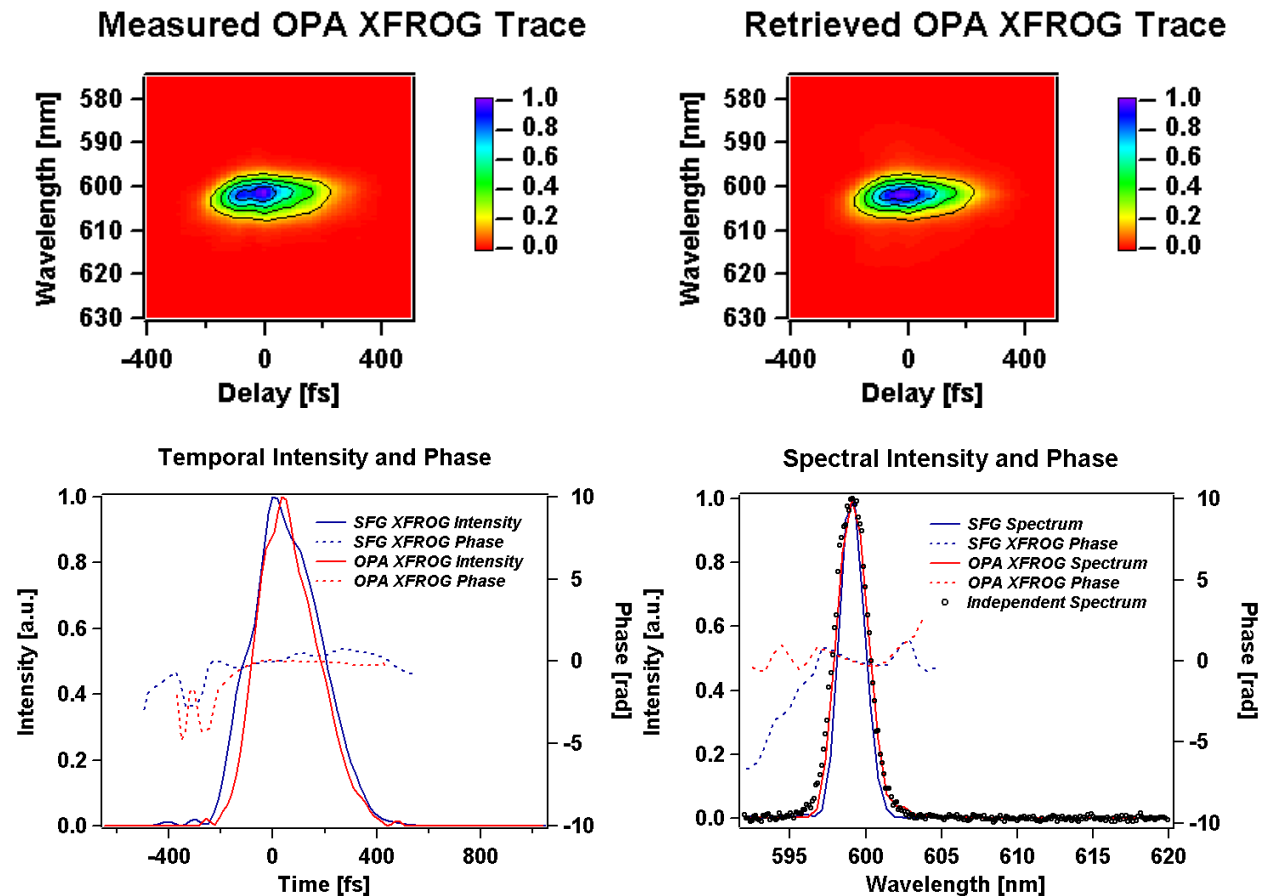
Spectral Intensity and Phase

Fig. 9. The measured and retrieved traces and retrieved intensity and phase vs. time and the spectrum and spectral phase vs. wavelength of a spectrally filtered continuum from a sapphire plate. The retrieved intensity and phase from the OPA XFROG measurement of 80 fJ pulses agrees well with the retrieved intensity and phase of unattenuated continuum of 80 pJ using the established technique, SFG XFROG.

Finally, using a NOPA geometry, we crossed the pump pulse and white light continuum at an angle of ~ 6.5° (internal in the crystal), chosen in order to minimize GVM. Using band-pass filters again we spectrally filtered the white light continuum, this time to a bandwidth of ~100 nm. We performed OPA XFROG measurements for two cases, as shown in Fig. 11. For the first OPA XFROG trace, the energy of the pulse was measured to be 500 pJ. The gain experienced in

this instance was ~ 50, which we considered the low gain condition. This pulse was then attenuated by four orders of magnitude to 50 fJ and its OPA XFROG trace measured again. This condition had a higher gain of ~1000. The intensity and phase from the two cases compared well, showing that higher gain did not distort the spectral phase during the OPA XFROG measurement process.
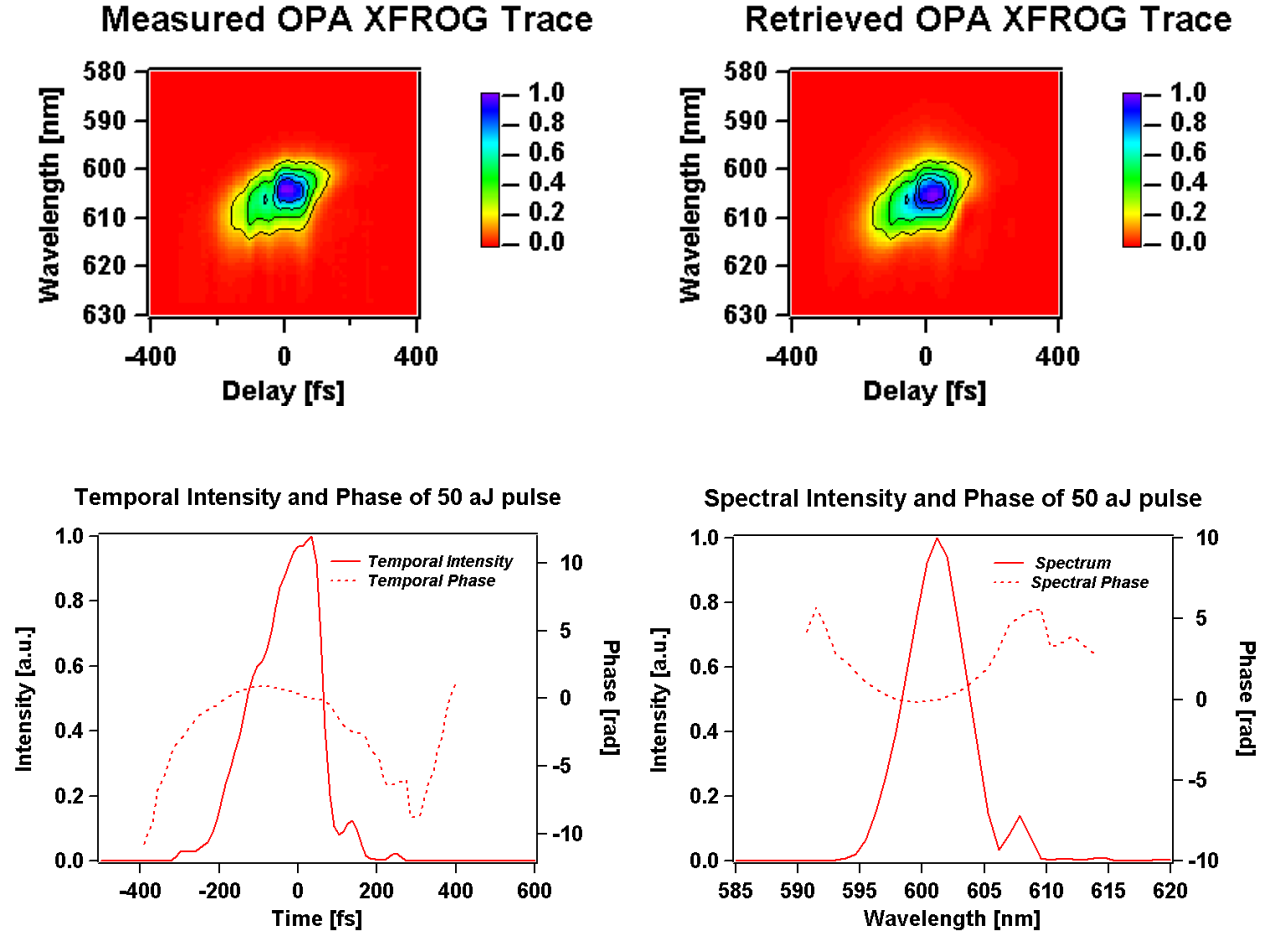

Fig. 10. OPA XFROG measurement of a 50 aJ attenuated and filtered continuum generated using a sapphire plate.

The Group Delay Mismatch (GDM) between the various frequencies of the unknown pulse and the pump pulse was calculated to be ~100 fs over the nearly 60 nm spectral envelope FWHM of an 860 fs long pulse. A thinner crystal would further reduce the GDM, but requiring a compromise on the gain that can be achieved. This sets a limitation on how weak a pulse can be measured. In this demonstration, we used a 2 mm-thick Type I OPA crystal, which was able to measure 50 fJ weak broadband pulses. Geometrical smearing effects in both the longitudinal and transverse directions were calculated to be 56 fs and 34 fs, respectively, for the non-collinear geometry.

As an aside, it must be pointed out that the structure in the white light continuum is real and is the nature of white light continuum generated by nonlinear optical processes, as discussed in the previous section. This structure would not be observed in spectral measurements using spectrometers for reasons discussed earlier. Another reason is that the white light continuum from the sapphire plate in these experiments was collected from multiple filaments in the spatially incoherent bulk-generated continuum, in order to duplicate the poor spatial behavior of

broadband fluorescence. So the spatial incoherence would also wash out the structure. Our OPA XFROG measurements retrieved a typical spectrum of the broadband continuum structure.

The experiments discussed above have all been performed using the OPA XFROG geometry. DFG XFROG should yield similar results with the same gain. Thus OPA/DFG XFROG promises to be a powerful new technique which opens up the field of pulse measurement to ultrafast and ultraweak, complex and broadband, arbitrary light pulses.
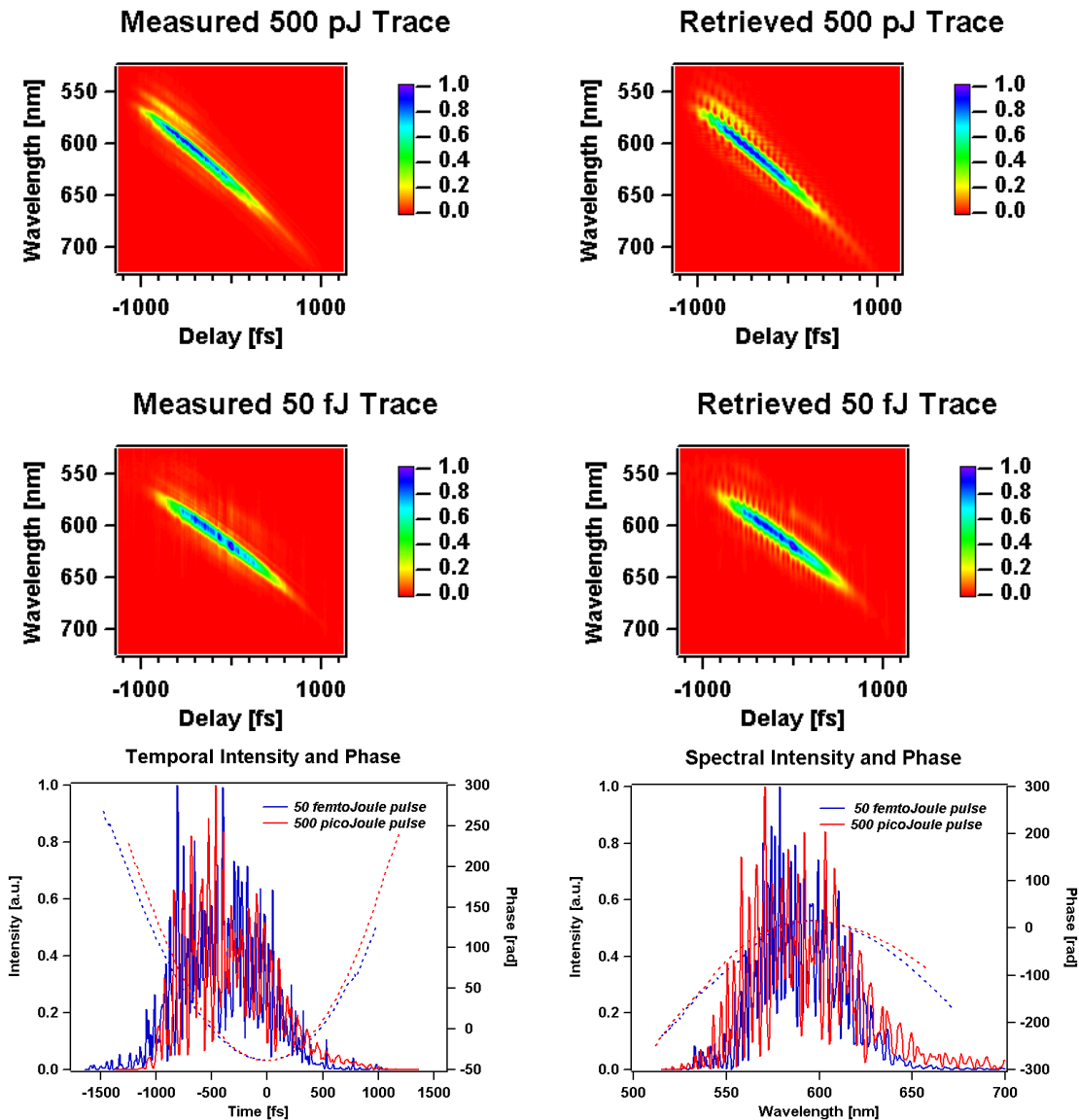
Fig. 11. OPA XFROG measurements of broadband white light continuum for cases of low gain in a 500 pJ strong pulse and high gain in a 50 fJ weak pulse.

Extremely Simple FROG Device: GRENOUILLE

While the above methods can measure very complex light pulses, they do not involve complex devices. However, if the pulse to be measured is a fairly simple laser pulse, then we might expect the device to be very simple. In fact, we recently showed that it is possible to

17

create a SHG FROG device for measuring ultrashort laser pulses that consists entirely of only four or five optical elements, and it is so simple that, once set up, it never requires realignment.

We call this simple variation GRENOUILLE (GRating-Eliminated No-nonsense Observation of Ultrafast Laser-Light E-fields).[2, 27] GRENOUILLE involves two innovations (see Fig. 12). First a Fresnel biprism replaces the beam splitter and delay line in a FROG, and second a thick crystal replaces the thin crystal and spectrometer in a FROG, yielding a very simple device.
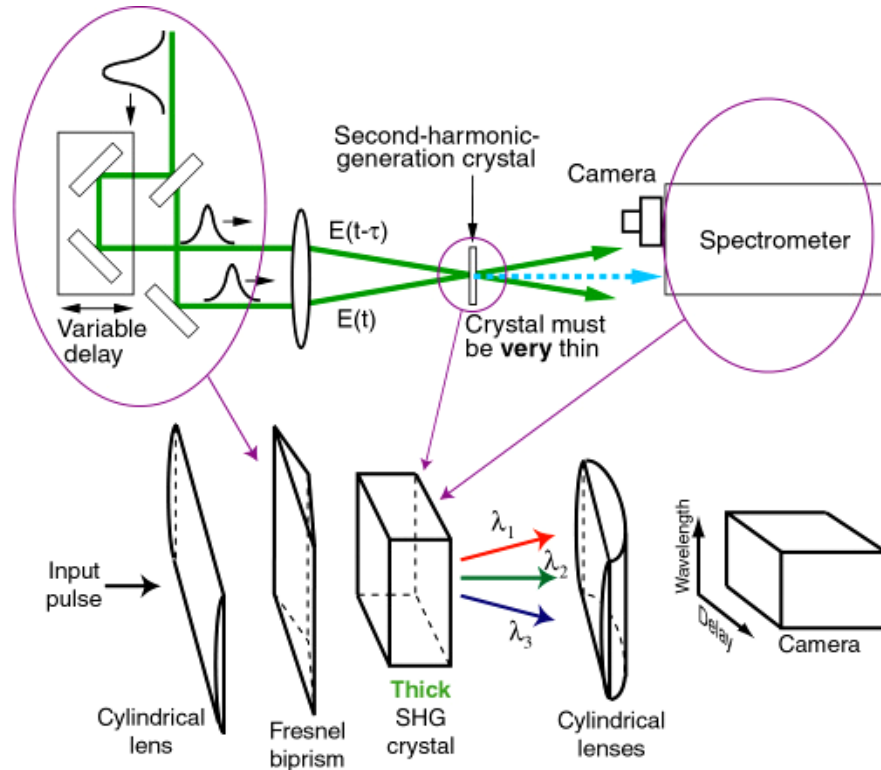
Fig. 12. FROG device (top) and the much simpler GRENOUILLE (bottom), which involves replacing the more complex components with simpler ones.

Specifically, when a Fresnel biprism (a prism with an apex angle close to 180°) is illuminated with a wide beam, it splits the beam into two and crosses these beamlets at an angle as in conventional single-shot autocorrelator and FROG beam geometries, in which the relative beam delay is mapped onto the horizontal position at the crystal (see Fig. 13). But, better than conventional single-shot geometries, the beams here are *automatically aligned* in space and in time, a significant simplification. Then, as in standard single-shot geometries, the crystal is imaged onto a CCD camera, where the signal is detected vs. position (i.e., delay) in the horizontal direction.

FROG also involves spectrally resolving the pulse after it has been time-gated by itself. GRENOUILLE (see Fig. 14) combines both of these operations in a single *thick* SHG crystal. As usual, the SHG crystal performs the self-gating process: the two pulses cross in the crystal with variable delay. But, in addition, the thick crystal has a very small phase-matching bandwidth, so the phase-matched wavelength produced by it varies with angle. Thus, the thick crystal also acts as a *spectrometer*. The first cylindrical lens must focus the beam into the thick crystal tightly enough to yield a range of crystal incidence (and hence exit) angles large enough to include the entire spectrum of the pulse. After the crystal, a cylindrical lens then maps the

crystal exit angle onto position at the camera, with wavelength a near-linear function of (vertical) position.

The resulting signal at the camera will be an SHG FROG trace with delay running horizontally and wavelength running vertically (see Fig. 15).
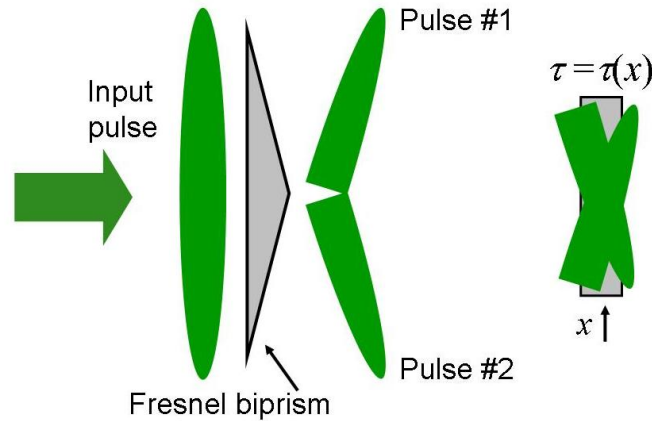

Fig. 13. Single-shot FROG measurements involve crossing large beams at a large angle, so that the relative delay between the two beams varies transversely across the crystal (left). This can be accomplished more easily and without the need for alignment using a prism with a large apex angle (right).
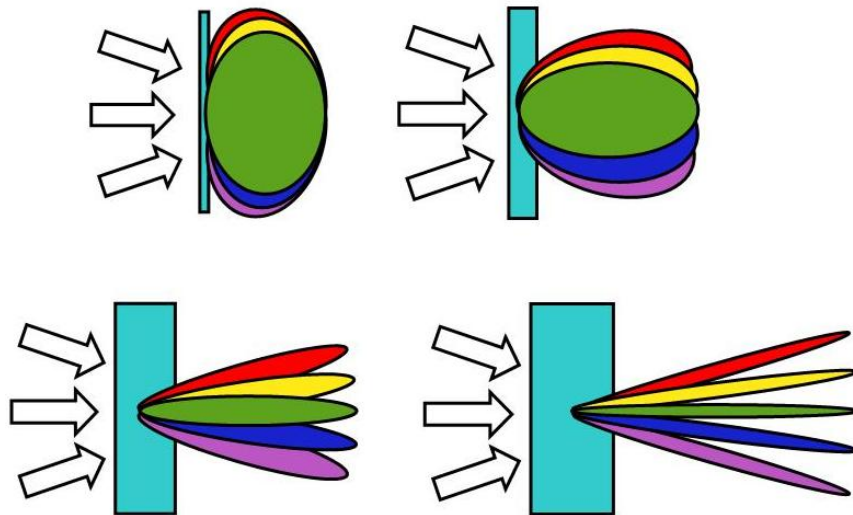
Fig. 14. Polar plots of SHG efficiency vs. output angle for various colors of a broadband beam impinging on a SHG crystal. Different shades of gray indicate different colors. Note that, for a thin crystal (upper left), the SHG efficiency varies slowly with angle for all colors, leading to a large phase-matching bandwidth for a given angle. As the crystal thickness increases, the polar plots become narrower, leading to very small phase-matching bandwidths. The thinnest crystal shown here would be required for all pulse-measurement techniques. GRENOUILLE, however, uses a thick crystal (lower right) to

spectrally resolve the autocorrelation signal, yielding a FROG trace — without the need for a spectrometer.

The key issue in GRENOUILLE is the crystal thickness. Ordinarily, achieving sufficient phase-matching bandwidth requires *minimizing* the group-velocity mismatch, GVM: the fundamental and the second harmonic must overlap for the entire SHG crystal length, *L*. This condition is: $GVM \cdot L \ll \tau_p$, where τ_p is the pulse length, $GVM \equiv 1/v_g(\lambda_0/2) - 1/v_g(\lambda_0)$, $v_g(\lambda)$ is the group velocity at wavelength λ, and λ_0 is the fundamental wavelength. For GRENOUILLE, however, the opposite is true; the phase-matching bandwidth must be *much less than* that of the pulse:

$$GVM \cdot L \gg \tau_p,$$

which ensures that the fundamental and the second harmonic *cease* to overlap well before exiting the crystal, which then acts as a frequency filter.
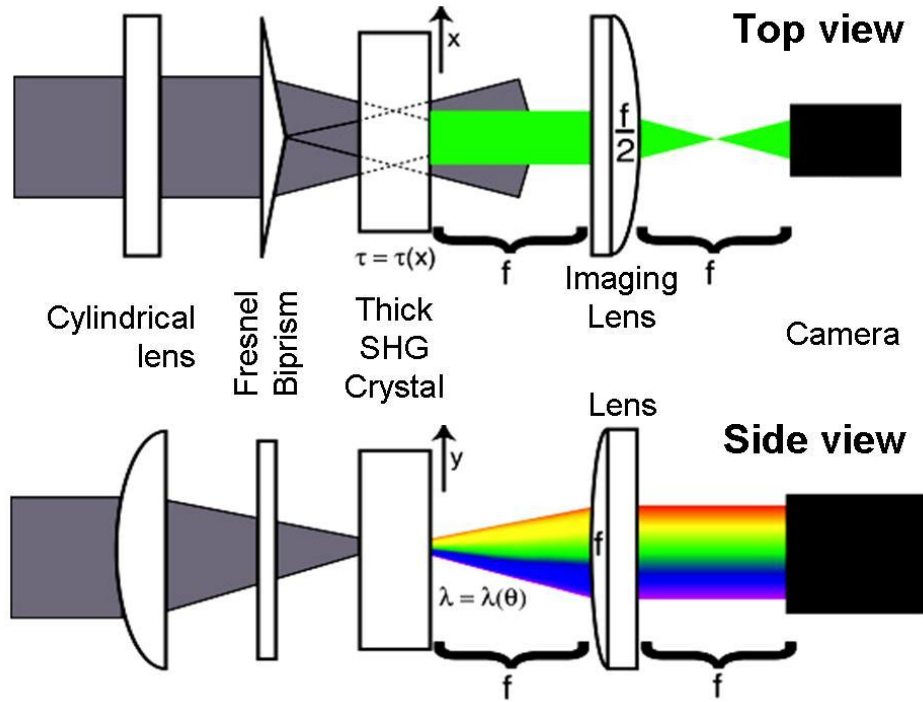

Fig. 15. Top and side views of GRENOUILLE.

On the other hand, the crystal must not be too thick, or group-velocity *dispersion* (GVD) will cause the pulse to spread in time, distorting it:

$$GVD \cdot L \ll \tau_c$$

where $GVD \equiv 1/v_g(\lambda_0 - \delta\lambda/2) - 1/v_g(\lambda_0 + \delta\lambda/2)$, $\delta\lambda$ is the pulse bandwidth, and τ_c is the pulse coherence time (~ the reciprocal bandwidth, $1/\Delta\nu$), a measure of the smallest temporal feature of the pulse. Since GVD < GVM, this condition is ordinarily already satisfied by the usual GVM condition. But here it will not necessarily be satisfied, so it must be considered. Combining these two constraints, we have:

$$GVD \, (\tau_p \, / \tau_c \,) \;\; << \;\; \tau_p \, /L \;\; << \;\; GVM$$

There exists a crystal length L that satisfies these conditions simultaneously if:

$$GVM \, / \, GVD \;\; >> \;\; TBP$$

where we have taken advantage of the fact that τ_p/τ_c is the TBP of the pulse. This equation is the fundamental equation of GRENOUILLE.
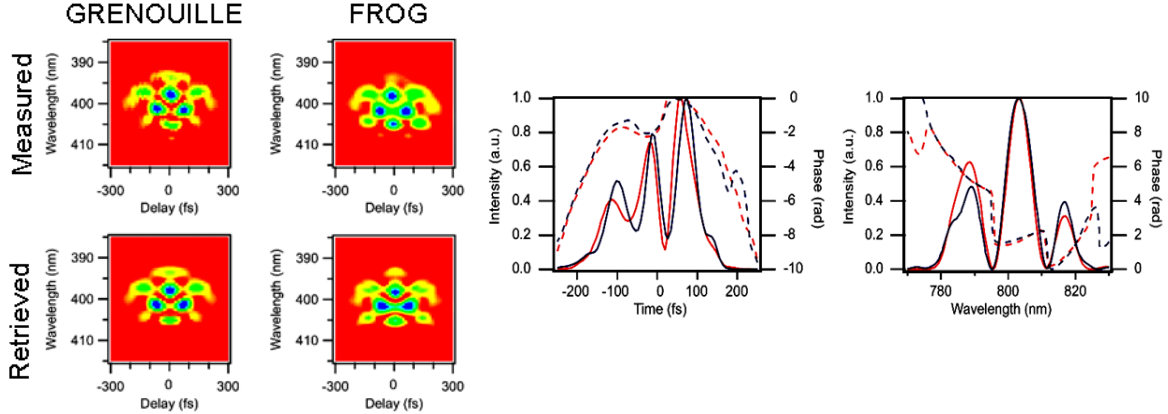

Fig. 16. GRENOUILLE and FROG measurements of the same pulse. Left: Measured and retrieved FROG and GRENOUILLE traces. Right: Retrieved intensity and phase vs. time for FROG (red) and GRENOUILLE (blue) measurements.

For a near-transform-limited pulse (TBP ~ 1), this condition is easily met because GVM >> GVD for all but near-single-cycle pulses. Consider typical near-transform-limited (i.e., $\tau_p \sim \tau_c$) Ti:Sapphire oscillator pulses of ~ 100 fs duration, where $\lambda_0 \sim 800$ nm, and $\delta\lambda \sim 10$ nm. Also, consider a 5 mm BBO crystal — about 30 times thicker than is ordinarily appropriate. In this case, the GRENOUILLE equation is satisfied: 20 fs/cm << 100 fs/0.5 cm = 200 fs/cm << 2000 fs/cm. Note that, for GVD considerations, shorter pulses require a thinner, less dispersive crystal, but shorter pulses also generally have broader spectra, so the same crystal will provide sufficient spectral resolution. For a given crystal, simply focusing near its front face yields an effectively shorter crystal, allowing a change of lens or a more expanded beam to "tune" the device for shorter, broader-band pulses. Less dispersive crystals, such as KDP, minimize GVD, providing enough temporal resolution to accurately measure pulses as short as 50 fs. Measurements of somewhat complex ~ 100 fs pulses are shown in Fig. 16. Conversely, more dispersive crystals, such as LiIO$_3$, maximize GVM, allowing for sufficient spectral resolution to measure pulses as narrowband as 4.5 nm (~200 fs transform-limited pulse length at 800 nm). Also, note that the temporal-blurring effect found in thick nonlinear media[2] is not found in the single-shot SHG geometry used by GRENOUILLE.

The main factor limiting GRENOUILLE's accurate measurement of shorter pulses is material-induced dispersion in the transmissive optics, including the necessarily thick crystal. Since shorter pulses have broader spectra, material dispersion is more significant and problematic. Another factor is that, for GRENOUILLE to work properly, the entire pulse spectrum must be phase-matched for some beam angle, requiring a large range of angles in the non-linear crystal. This can be accomplished using a tighter focus, but then the resulting shorter confocal parameter of the beam reduces the effective crystal length that can be used, reducing spectral resolution.

Fortunately, these problems can be solved by designing a tighter focused, nearly-all-reflective GRENOUILLE, which can measure 800 nm laser pulses as short as 20 fs.[41] We convert almost all the transmissive components to reflective ones, except the Fresnel biprism (~ 1.3 mm of fused silica). This eliminates most of the material dispersion that would be introduced by the device. Moreover, the "thick" crystal required to spectrally resolve (using phase-matching) a 20 fs pulse is also thinner: only 1.5 mm. This not only allows us to eliminate dispersion induced by crystal, but also allows us to focus tighter (this yields a shorter beam confocal parameter, decreasing the effective nonlinear interaction length), covering the spectra of short pulses. This is important because the device must be able to measure pulses with bandwidths of ~ 50 nm, that is, the device should have ~ 100 nm of bandwidth itself. The short interaction length in the crystal reduces the device spectral resolution, but fortunately, due to their broadband nature, shorter pulses require less spectral resolution. With these improvements, a GRENOUILLE can be made that is as simple and as elegant as the previously reported device, but which is capable of accurately measuring much shorter pulses: 20 fs or shorter.

To test the reliability of our short-pulse GRENOUILLE, we used a Ti:Sapphire oscillator operating with ~ 60 nm (FWHM) of bandwidth, and we used an external prism pulse compressor to compress the pulse as much as possible. We measured the output pulse with conventional multi-shot FROG and with our GRENOUILLE. We then used the Femtosoft FROG code to retrieve the intensity and phase for both measurements. Figure 16 shows measured and retrieved traces as well as the retrieved intensity and phase for multi-shot FROG and GRENOUILLE measurements, all in excellent agreement with each other. The pulse that GRENOUILLE retrieved in these measurements is 19.7 fs FWHM.
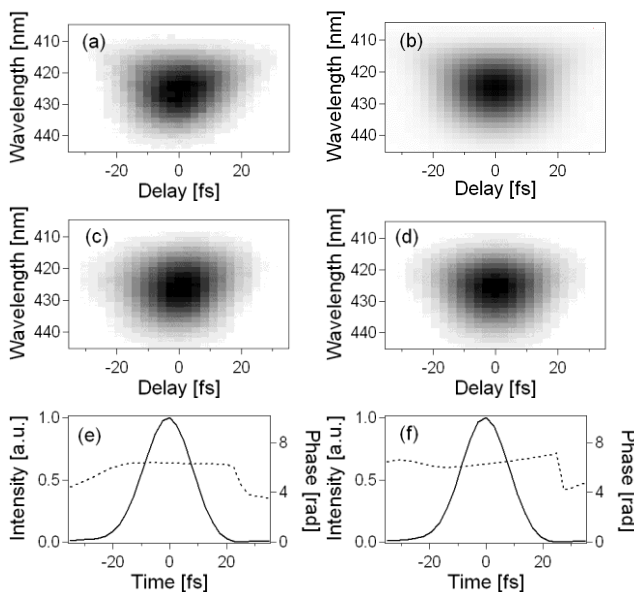

Fig. 17. Comparisons of short-pulse GRENOUILLE and multi-shot FROG measurements. (a) Measured GRENOUILLE trace. (b) Measured multi-shot FROG trace. (c) Retrieved GRENOUILLE trace. (d) Retrieved multi-shot FROG trace. (e) Retrieved intensity and phase vs. time for GRENOUILLE measurements (temporal pulse width 19.7 fs FWHM). (f) Retrieved intensity and phase vs. time for multi-shot FROG measurements (temporal pulse width 19.4 fs FWHM)

Because ultrashort laser pulses are routinely dispersed, stretched, and (hopefully) compressed, it is common for them to contain spatio-temporal distortions, especially spatial chirp (in which the average wavelength of the pulse varies spatially across the beam) and pulse-front tilt (in which the pulse intensity fronts are not perpendicular to the propagation vector).

Unfortunately, convenient measures of these distortions have not been available. Fortunately, we have recently shown that GRENOUILLE and other single-shot SHG FROG devices automatically measure both of these spatio-temporal distortions.[29, 30] And they do so without requiring a single alteration in the setup!

Specifically, spatial chirp introduces a shear in the SHG FROG trace, and pulse-front tilt displaces the trace along the delay axis. Indeed, the single-shot FROG or GRENOUILLE trace shear is approximately *twice* the spatial chirp when plotted vs. frequency and *one half* when plotted vs. wavelength (Fig. 18). Pulse-front tilt measurement involves simply measuring the GRENOUILLE trace displacement (Fig. 17). These trace distortions can then be removed and the pulse retrieved using the usual algorithm, and the spatio-temporal distortions can be included in the resulting pulse intensity and phase.
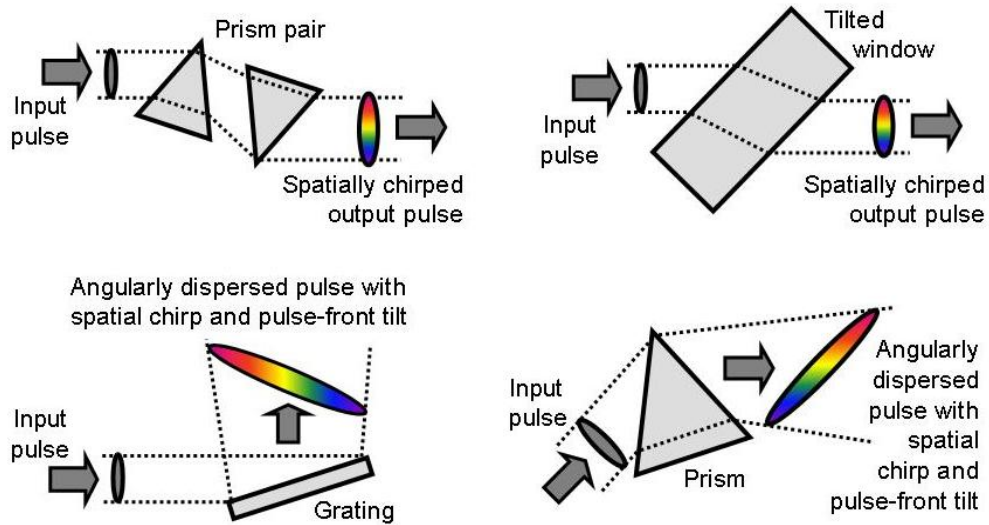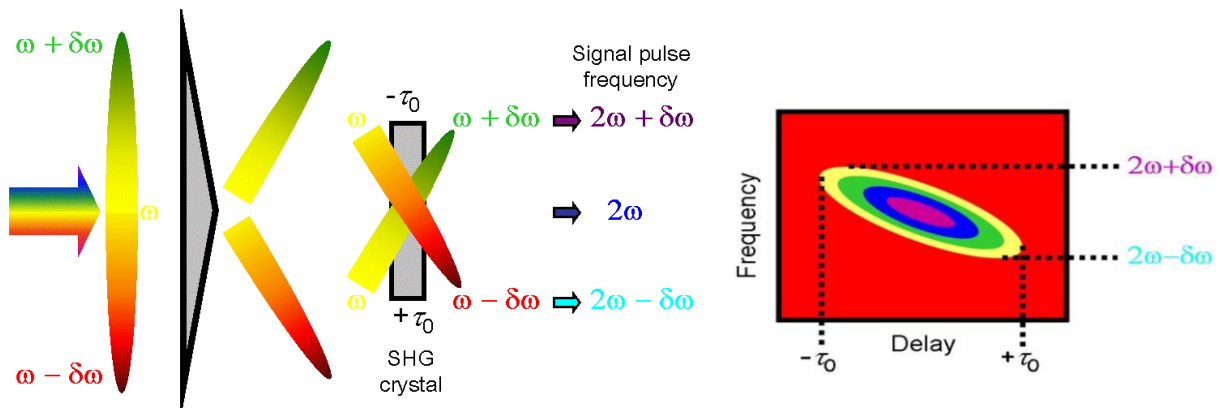

Fig.18. Spatio-temporal distortions. Top: spatial chirp. Bottom: Spatial chirp and pulse-front tilt.
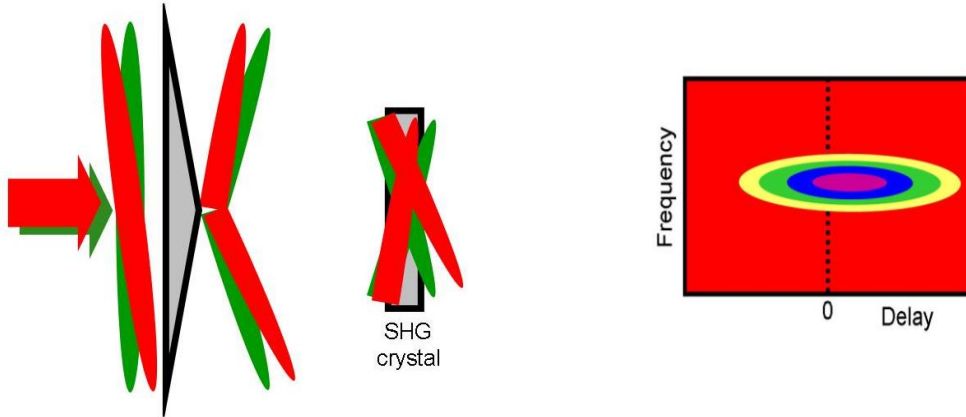
Fig. 19. Spatial chirp tilts (shears) the trace (above), and pulse-front tilt translates the trace in delay (below) in GRENOUILLE measurements. This allows GRENOUILLE to measure these distortions easily and without modification to the apparatus.

We have also made independent measurements of spatial chirp by measuring spatio-spectral plots (i.e., spatially resolved spectra), obtained by sending the beam through a carefully aligned imaging spectrometer (ordinary spectrometers are not usually good diagnostics for spatial chirp due to aberrations in them that mimic the effect) and spatially resolving the output on a 2D camera, which yields a tilted image (spectrum vs. position) in the presence of spatial-chirp. We find very good agreement between this measurement of spatial chirp and that from GRENOUILLE measurements.
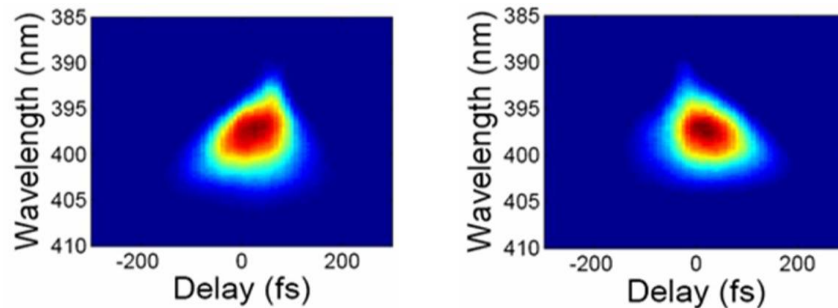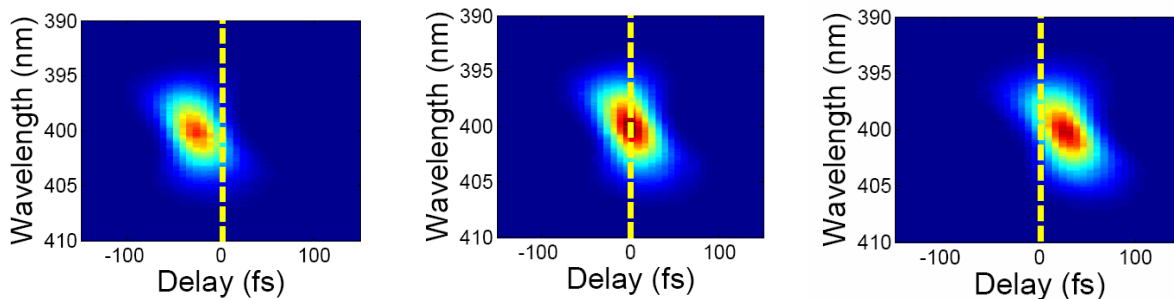

Fig. 20. Experimental GRENOUILLE traces for pulses with positive (left) and negative (right) spatial chirp. The tilt in GRENOUILLE traces reveals the magnitude and sign of spatial chirp.

To vary the pulse-front tilt of a pulse, we placed the last prism of a pulse compressor on a rotary stage. By rotating the stage we were able to align and misalign the compressor, obtaining positive, zero, or negative pulse-front tilt. Figure 21 shows theoretical and experimental values
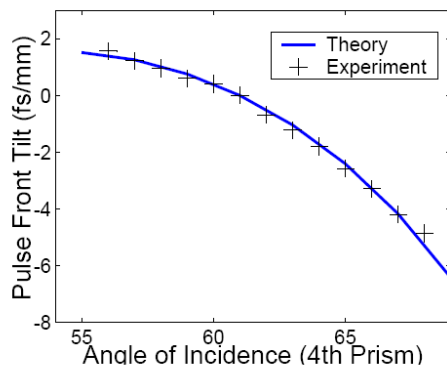

24

Fig. 21. Top: Measured GRENOUILLE traces for pulses with negative, zero, and positive pulse-front tilt (note that spatial chirp is also present in all these traces). The horizontal trace displacement is proportional to the pulse-front tilt. Below: Theoretically predicted pulse-front tilt and the experimentally measured pulse-front tilt using GRENOUILLE.

of pulse-front tilt in our experiments (right) and some experimental GRENOUILLE traces for different amounts of pulse-front tilt (left). We find very good agreement between theoretical values of pulse-front tilt and that from GRENOUILLE measurements.

GRENOUILLE not only measures the magnitudes of these two spatio-temporal distortions, but it also measures their sign. GRENOUILLE can, in principle, also measure all odd orders of the spatial chirp, although this additional power is not yet of great interest.

The ability to measure spatio-temporal distortions easily is already proving useful: we've found that most commercial ultrafast amplifiers emit beams with both spatial chirp and pulse-front tilt. And we've found that pulse-front tilt is present, not only in beams with angular dispersion (as is commonly believed), but also in beams with both spatial and temporal chirp, but no angular dispersion.

Measuring Shaped Pulses: SEA TADPOLE

Many applications of ultrashort pulses, from coherent control [42, 43] to multi-photon microscopy[44, 45], utilize very complicated shaped pulses. To optimize these experiments, it is important to be able to completely characterize these complicated pulses. Also, such experiments often require the use of feedback loops to select the appropriate pulse shape, and usually pulse measurement is a necessary part of these loops. Therefore a fast (video-rate) pulse-measurement technique for measuring shaped pulses would benefit coherent control experiments.

Only three techniques have proven capable of measuring complex pulses: frequency-resolved-optical gating (FROG)[2], cross-correlation FROG (XFROG)[33], and (linear) spectral interferometry (SI). FROG techniques, while quite fast for simple pulses (time-bandwidth product $< \sim 10$), can be slow when the pulse is complex (> 1 s for convergence). SI has the advantage that it is inherently a single-shot technique, and the interferogram can be directly and quickly inverted regardless of the complexity of the pulse. Therefore SI could in principle be used to measure very complicated pulses in real-time. Another useful property of SI is that it is a linear technique, and so it is extremely sensitive and can measure pulses that are approximately nine orders of magnitude weaker than those that can be measured using nonlinear-optical methods.[46] SI's only fundamental drawback is that it requires a previously measured reference pulse whose spectrum contains that of the unknown pulse. Fortunately, when measuring shaped pulses, the unshaped pulse provides an ideal such reference pulse, and it is easily measured using another technique, such as FROG or its experimentally simpler version, GRENOUILLE.

Unfortunately, traditional SI has a few practical limitations that have prevented it from working well for this application. The standard reconstruction algorithm for SI, often referred to as FTSI, (Fourier Transform Spectral Interferometry) involves introducing a delay between the interfering pulses and then Fourier filtering the data along the time-axis. Reconstructing the field in this way results in a loss of spectral resolution typically by a factor of about five. Thus, very bulky (~ 1 m) high-resolution spectrometers are required for measuring the longer shaped pulses (which can be as long as 10 ps). Another important practical problem with SI is that it has extremely strict alignment requirements, such as perfectly collinear beams with similar intensities and identical spatial modes, so its alignment must be frequently tweaked. SI would be very useful for measuring shaped pulses if these two problems could be overcome.

Fortunately, it is possible to overcome the loss of resolution experienced with FTSI by crossing the pulses at an angle to yield interference fringes versus position, x_c,[47-52] and measuring a 2-D interferogram versus camera position (x_c) and wavelength (λ). In this device, the pulses are temporally overlapped, so that no additional spectral resolution is required. In this case, the measured interferogram $I(x_c,\lambda)$ is given by:

$$S(\lambda, x_c) = S_{ref}(\lambda) + S_{unk}(\lambda)$$
$$+2\sqrt{S_{ref}(\lambda)}\sqrt{S_{unk}(\lambda)}\cos(2\mathrm{k}x_c\sin\theta + \varphi_{unk}(\lambda) - \varphi_{ref}(\lambda))$$

The spectral intensity and phase of the unknown pulse can then be retrieved by Fourier filtering the interferogram along the x_c axis, and, as a result, the unknown pulse is reconstructed with the full resolution of the spectrometer[47].

We recently introduced an interferometer based on this idea, which we call SEA TADPOLE or Spatially Encoded Arrangement for Temporal Analysis by Dispersing a Pair of Light E-Fields.[23-25] In SEA TAPDOLE, in addition to reconstructing the unknown field with the full resolution of the spectrometer, we also use a simple experimental set-up (using optical fibers) that makes the device very insensitive to misalignments and easy to use. Using SEA TAPDOLE we have shown that pulses with time bandwidth products (TBP) as large 400 could be measured, and others have since shown that SEA TAPDOLE is useful for measuring shaped pulses[53]. Additionally, we even found that, for many pulses, the spectrum that we retrieve from the interferogram is better resolved than the spectrum that we measure directly with the spectrometer in SEA TAPDOLE, and this improvement can be as great as a factor of 7 (in the sense that the spectral fringe contrast was 7 times better in the SEA TAPDOLE spectrum).[23]
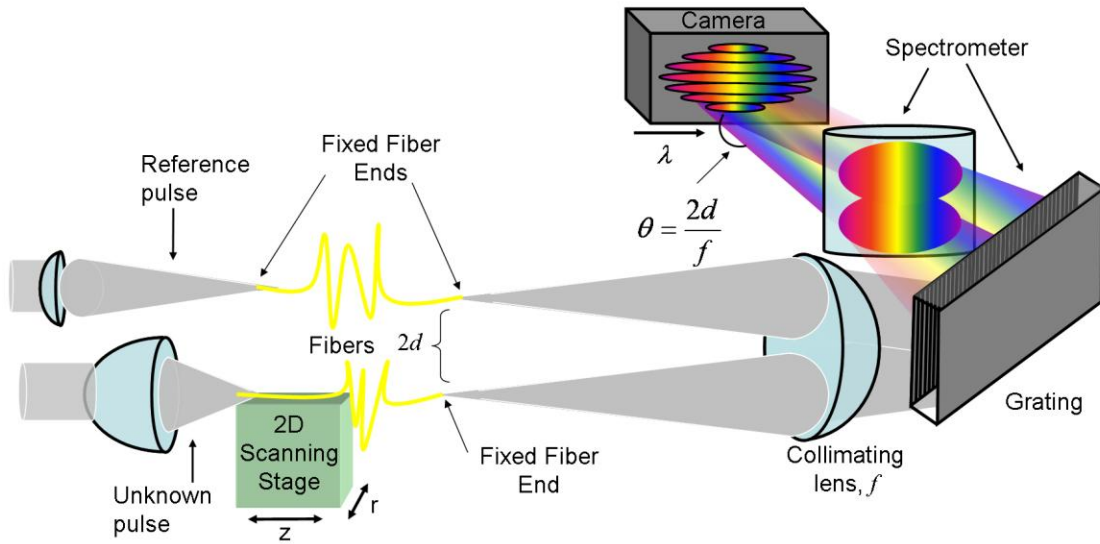
Fig. 22. SEA TADPOLE Experimental Setup (color online only): A reference pulse and an unknown pulse are coupled into two single-mode fibers with approximately equal lengths. At the other end of the fibers, the diverging beams are collimated using a spherical lens (*f*). After propagating a distance *f*, the collimated beams cross and interfere, and a camera is placed at this point to record the interference. In the other dimension, a grating and a cylindrical lens map wavelength onto the camera's horizontal axis (x_c).

To measure $E_{unk}(\lambda)$ using SEA TAPDOLE, we couple the reference and unknown pulses into two identical fibers. The output ends of the fibers are placed close together, so that when the light diverges from them, both beams are collimated with the same spherical lens (focal length f). Because the fibers are displaced from the optic axis (with a distance d between them which is usually <1mm) the collimated beams cross at angle θ which is equal to d/f and we place a camera at the crossing point in order to record their interference. In the other dimension we use a diffraction grating and a cylindrical lens to map wavelength onto horizontal position (as in a conventional spectrometer) so that we record a two-dimensional interferogram. Figure 22 illustrates the experimental setup. Note that, when we are using SEA TAPDOLE to measure $E_{unk}(\lambda)$ of a pulse that is free of spatio-temporal couplings, the scanning stage shown in Typical experimental parameters include a crossing angle of 0.06 degrees, a camera with about 10^6 pixels, each 4.7 μm^2 in area, a collimating lens with a focal length of 150 mm, 40-cm long fibers with a mode size of 5.3 μm, and we typically build the spectrometer to have a range of 80 nm and a spectral resolution of about 0.14 nm (as we will show later). The range of the wavelength axis can be decreased in order to increase the spectral resolution simply by using a longer focal length cylindrical lens, as in any spectrometer, and the usual limitations of grating spectrometers apply.
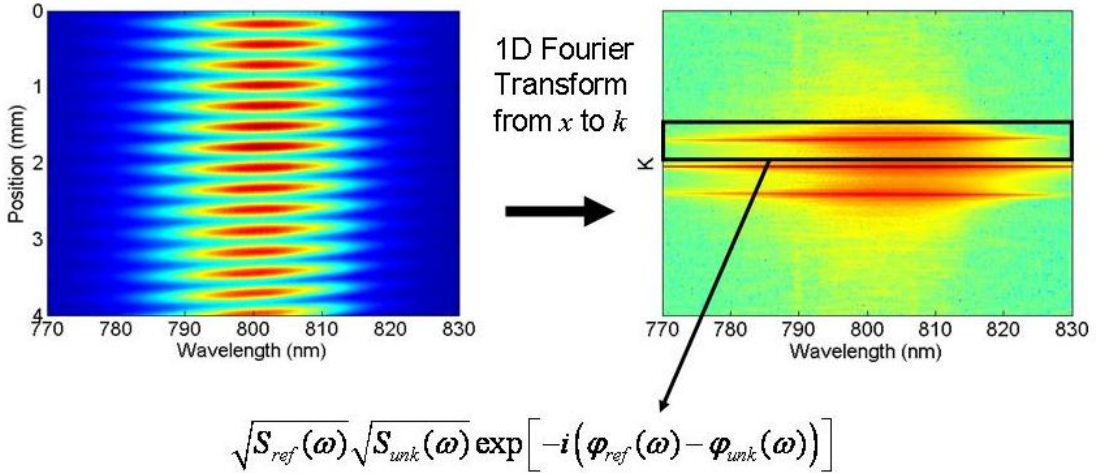

$$\sqrt{S_{ref}(\omega)}\sqrt{S_{unk}(\omega)}\exp\left[-i\left(\varphi_{ref}(\omega)-\varphi_{unk}(\omega)\right)\right]$$

Fig. 23. SEA TADOLE retrieval. The top left image is a typical interferogram, which is Fourier transformed from the λ-x_c to the λ-k_c domain where only one of the sidebands is then used. This sideband is then inverse-Fourier transformed back to the λ-x domain. The result is then averaged over x_c and the reference pulse is divided out in order to isolate the intensity and phase of the unknown pulse.

The only requirements on the reference pulse in SEA TAPDOLE are that it be from the same laser, so that the interfering pulses are coherent (time-synchronized), and its spectrum must contain that of the unknown pulse (otherwise the spectral-interference term is zero at that frequency). The best reference pulse is generally the pulse taken directly from the laser because this is usually a spatially and spectrally smooth pulse that does not complicate the SEA TADPOLE measurement[54]. If it is only necessary to determine the phase and spectrum introduced by an experiment such as some material, a lens, or a pulse shaper, then it is not necessary to characterize the reference pulse.

There is no direction of time ambiguity in SEA TADPOLE. If the unknown pulse enters the device from the bottom fiber, then the phase difference will have the sign shown in the above equation, and it will have the opposite sign if the unknown pulse enters through the top fiber. It is also necessary to consider which interference term (in our analysis we used the top one) is used in the reconstruction because these are complex conjugates of one another so their spectral phase differences have opposite signs.

We have used SEA TADPOLE to measure a variety of complex shaped pulses. Here, we describe a phase-shaped pulse, shaped using a 256-element LCD pulse shaper. For this experiment, we used an 85MHz repetition rate KM labs Ti:Sapphire oscillator, which had approximately 30 nm of bandwidth. For the reference pulse, we used the unshaped oscillator pulse so that the phase difference that we measured with SEA TAPOLE was the phase introduced by the pulse shaper. Figure 24 shows the results of this experiment. Figure 24b shows the phase that was applied by the shaper and the phase that was measured by SEA TAOPOLE and you can see that the two are in good agreement. Figure 24c shows the reconstructed spectrum ($S_{unk}(\lambda)$) compared to the spectrometer measurement ($S_{sp}(\lambda)$) where $S_{sp}(\lambda)$ was measured using the spectrometer in SEA TADPOLE by blocking the reference pulse. You can see that $S_{unk}(\lambda)$ is essentially a *better resolved* version of $S_{sp}(\lambda)$ as is often the case in SEA TAPDOLE. Figure 24d shows the reconstructed temporal field and you can see that this pulse had a TBP of around 100. Figure 24a is the SEA TAPDOLE trace and it nicely illustrates that the curvature of the fringes is the phase difference between the interfering pulses.
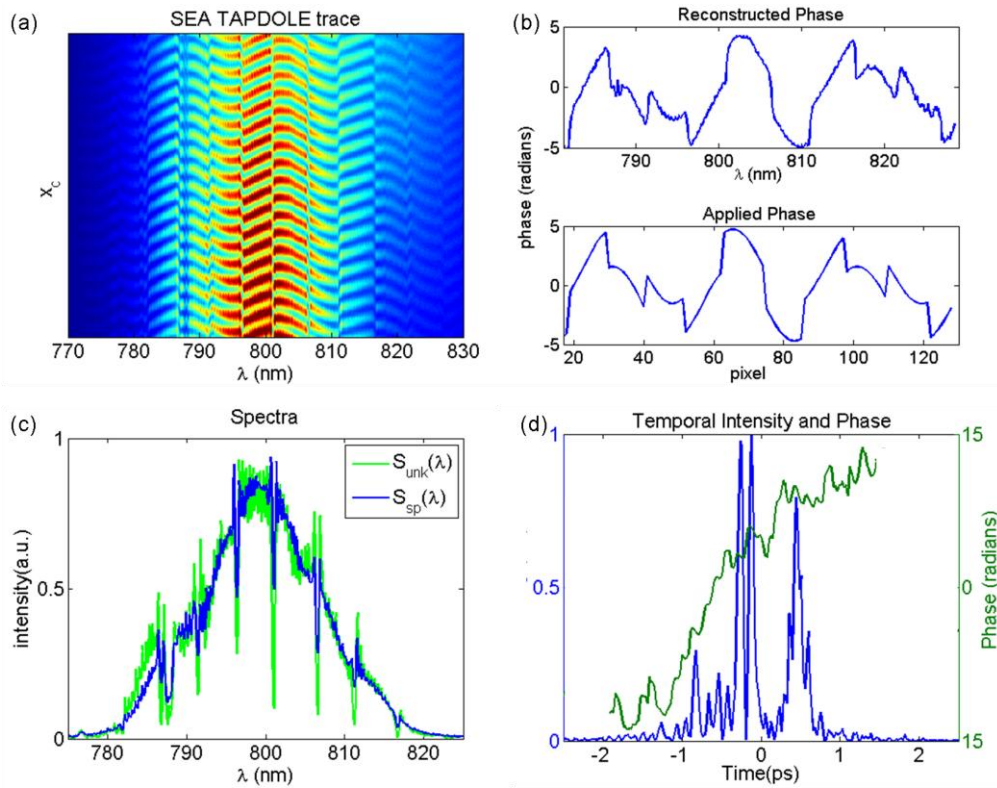

Fig. 24. (a) SEA TADPOLE trace for a shaped pulse. (b) The retrieved spectral phase compared to the shaper-applied phase. (c) The retrieved spectrum (S_{unk}, green) compared to the spectrometer spectrum (S_{sp}, blue). (d) the retrieved temporal intensity and phase.

Measuring the Complete Spatio-temporal Field of Even Focused Pulses: SEA TADPOLE

Nearly all ultrashort pulses are utilized at a focus, where their intensity is high. And in addition to their possible complexity in time and frequency, focused pulses can easily have complex spatio-temporal structure, especially if lens aberrations are present [55-58]. Simulations have shown that it is difficult, if not impossible, to avoid group delay dispersion and pulse lengthening due to lens or curved-mirror aberrations, which result in radially varying group delay for example. When such distortions are present, adequate material dispersion

compensation is very difficult, and the pulse will not have a transform-limited pulse duration even with perfect material-dispersion compensation. This is especially important in fields such as nonlinear microscopy and micro-machining. Because the focus can easily contain such spatio-temporal distortions (and severe ones at that), simply making a measurement of the time- or frequency-dependent spectral intensity and phase is not a sufficient characterization of the pulse; a complete *spatio-temporal* measurement must be made at the focus. And because the pulse can be complex in both space and frequency (time), the measurement technique must have both high spatial and high spectral resolution.
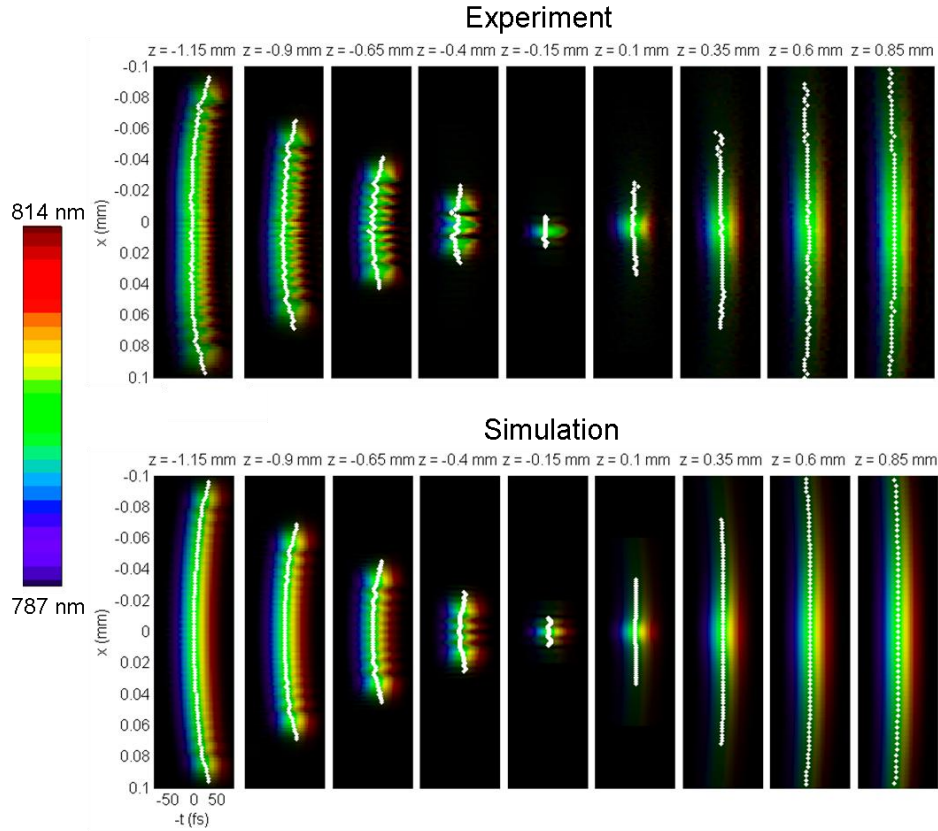

Fig. 25. *E(x,z,t)* in the focal region of a plano-convex lens. The experimental results are displayed in the top plots, and the simulations are shown in the bottom plots. Each box displays the amplitude of the electric field versus *x* and *-t* at a distance *z* from the geometric focus. The white dots show the pulse fronts, or the maximum temporal intensity for each value of *x*. The color represents the instantaneous frequency which shows that the redder colors are ahead of the bluer colors due to material dispersion.

Previous pulse measurement techniques have only been able to measure the focused pulse versus time averaged over space or vice versa [59-61]. With two-dimensional spectral interferometry it is possible to measure the spatio-temporal field of the recollimated focused pulse (by double passing the focusing lens), and this information can be used to numerically back-propagate the focused pulse to determine the spatio-temporal field at the focus by dividing the measured phase by 2. Drawbacks to this approach are that the pulse must be perfectly recollimated, it is difficult to measure aberrations due to misalignment of the lens, and the method is quite indirect: one has to assume that the numerical back propagation is correct[62].

Recently we demonstrated that SEA TAPDOLE can also be used to directly measure the spatio-temporal field of focusing ultrashort pulses.[23] Because the entrance to SEA TAPDOLE is a single-mode fiber, it naturally measures pulses with high spatial resolution, and the measurement can be made at the focus. If we use a fiber with a mode size smaller than the focused spot size, then we can make multiple measurements of $E_{unk}(\lambda)$ longitudinally and transversely, so that we measure $E_{unk}(x, y, z, \lambda)$ at and around the focus.

When using SEA TAPDOLE to measure the spatio-temporal field, $E_{unk}(x, y, z, \omega)$, the scanning stage shown in Figure 22 is used to move the entrance to the unknown pulse's fiber transversely and longitudinally so that multiple interferograms are measured all along the cross section and length of the incoming beam. This allows us to reconstruct $E_{unk}(\lambda)$ versus x, y, and z near the focal region, so that the spatio-temporal field of the focusing beam, $E_{unk}(x, y, z, \lambda)$ can be reconstructed. As we will discuss later, the spatial resolution of scanning SEA TAPDOLE, or the tightest focus that SEA TADPOLE can measure with a given fiber, is given by the NA of the fiber.

We measured $E_{unk}(x, \lambda)$ at nine different longitudinal positions (z) in the focal region produced by a BK7 lens with a focal length of 25 mm. The NA of the focus was 0.085 (using the $1/e^2$ full width of the beam before the lens). The input pulse had a bandwidth of 30 nm (FWHM), and we used a KM labs Ti:Sa laser with a center wavelength of 800nm. To verify that this measurement was correct, we propagated a Gaussian pulse through a lens using the experimental parameters listed above. For the numerical propagation, we used the Fresnel approximation to Huygens integral, which is valid for numerical apertures less than 0.1. Figure 25 displays the results of this experiment.
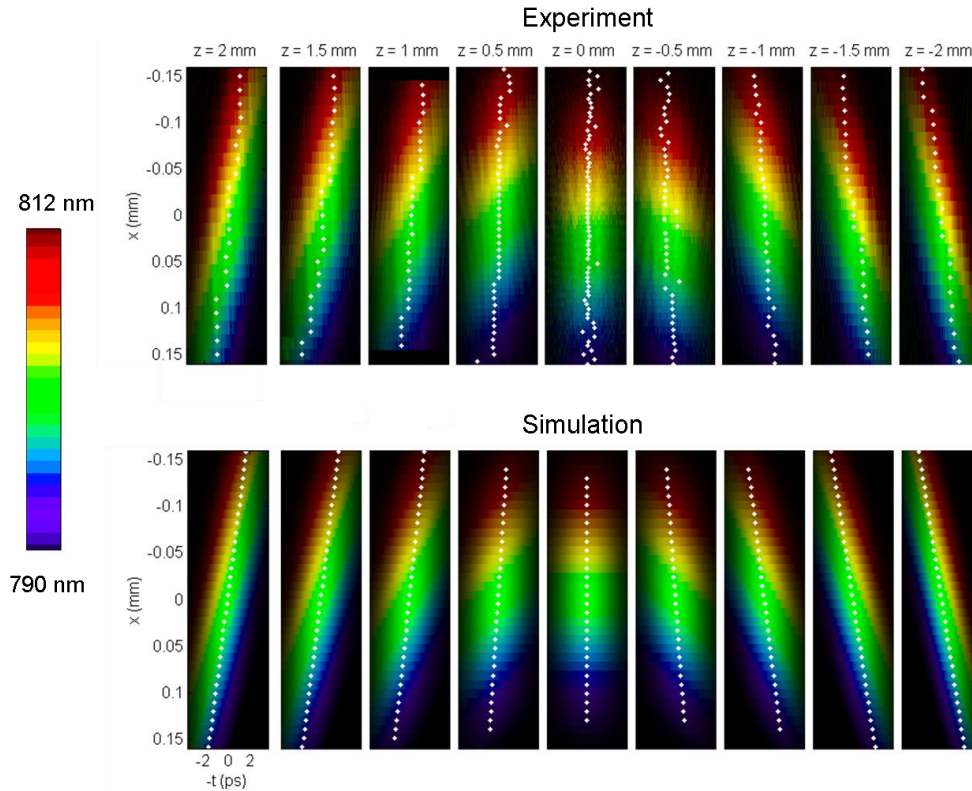

Fig. 26. *E(x,z,t)* in the focal region of beam which had angular dispersion. The angular dispersion becomes purely spatial chirp at the focus because a lens is a Fourier transformer.

The ripples before the focus are due to the spherical aberrations introduced by the lens. This lens also has chromatic aberrations present which cause the pulse fronts to be asymmetric about the focus. The color in the plots displays the instantaneous frequency (see the color bar in Fig. 25), and it shows that the redder colors are ahead of the bluer colors which is due to the material dispersion of the lens. While there should be some color variation due to chromatic aberrations, this is not noticeable because it is much smaller than that due to GDD. The aberrations in this lens increase the focused spot size by a factor of 3.

To further demonstrate scanning SEA TADPOLE, we focused a beam with angular dispersion and then measured the spatio-temporal field in at and around the focus. To introduce angular dispersion we used the -1 order of a ruled reflection grating (300 g/mm), which we placed just before (by 17.5 cm) the focusing lens.   We also simulated this experiment by calculating $E_{unk}(x, \lambda)$ just before the lens using Kostenbauder matrices and then numerically propagated this beam through the lens and to the focal region just as described above. The results of this experiment are shown in Fig. 26. Again, the experiment and simulation are in good agreement. Because a lens is a Fourier transformer, the angular dispersion introduced by the grating becomes spatial chirp at the focus. As a result, the pulse front becomes flat at the focus, because the pulse front tilt in this case is due to angular dispersion. Because the magnification of the optical system becomes negative after the focus, the order of the colors and the sign of the pulse front tilt change after the focus. This measurement essentially shows the pulse in the focal region of a spectrometer.   The lens used in this experiment is the aspheric lens described in reference[23].

Measuring Complex Pulses in Time and Space *on a Single Shot*: STRIPED FISH

Many laser systems operate at a very low repetition rate or have much shot-to-shot jitter and so require single-shot diagnostics. Unfortunately, most single-shot pulse-measurement techniques monitor the laser output either temporally or spatially only, and independent spatial and temporal measurements fail to capture possible spatio-temporal distortions[57, 63-71] because diagnostic devices for measuring the temporal behavior of the pulse usually integrate over the spatial transverse coordinates, and vice-versa.

To solve this problem, we have modified a method we have developed previously for measuring the complete spatio-temporal field of a laser pulse, $E(x,y,t)$, using wavelength-scanning digital holography.[72] In this method, digital holograms are captured sequentially as the wavelength of a reference laser beam is scanned across the bandwidth of the pulse under test. The spatial field at each frequency ω_k, $E(x,y;\omega_k)$, is obtained by numerical processing of individual digital holograms in the usual manner,[73] and a measurement of the spectral phase using frequency-resolved optical gating (FROG)[74] completes the measurement. All the information needed to reconstruct $E(x,y,t)$ is obtained since the temporal field can be simply calculated by an inverse Fourier transform:

$$E(x, y, t) = \frac{1}{2\pi} \sum_{\omega_k} E(x, y; \omega_k) \exp(i\omega_k t) \, \delta\omega$$

However, the scan of the wavelength requires multiple frames of data to be recorded. This, in turn, requires a stable train of identical pulses. To overcome this limitation, we recently introduced a device capable of measuring the complete three-dimensional spatio-temporal electric field $E(x,y,t)$ *on a single shot*. Instead of recording multiple digital holograms for different wavelengths sequentially in time, we record them simultaneously in a larger two-dimensional camera frame. This large digital hologram contains all the necessary information to numerically reconstruct the full three-dimensional electric field $E(x,y,t)$. For that reason, we call

our technique Spatially and Temporally Resolved Intensity and Phase Evaluation Device: Full Information from a Single Hologram (STRIPED FISH).[21, 22, 72]

Optical arrangements for simultaneously recording a few holograms have been introduced in the past, but these either involve numerous beam-splitters or a special cavity to generate a few replicas that must all be precisely synchronized[75]. As a result, they do not scale very well as the pulse becomes more complex in time (or frequency) and the number of necessary holograms increases. STRIPED FISH, on the other hand, is based on a simple concept comprising only a few optical components that readily generate a large number of spectrally-resolved holograms.

Recall how off-axis digital holography may be used to reconstruct the spatial electric field $E(x,y)$ of a monochromatic laser beam[76]. The "signal" beam (the beam to be characterized) and a "reference" beam (a pre-characterized beam) are crossed at a small angle α, for example, in the vertical plane. One then measures the corresponding intensity $I(x,y)$, or "digital hologram," using a digital camera:

$$I(x, y) = \left|E_s(x, y)\right|^2 + \left|E_r(x, y)\right|^2$$
$$+ E_s(x, y)^* E_r(x, y) \exp(-iky\sin\alpha) + E_s(x, y) E_r(x, y)^* \exp(+iky\sin\alpha)$$

Due to the crossing angle and the resulting spatial fringes, the last term of the above equation, which contains the complete spatial field of the signal beam, can be readily extracted from the measured intensity $I(x,y)$ using a well-established Fourier-filtering algorithm[73]. Assuming that the electric field of the reference beam ($E_r(x,y)$) is known, the spatial electric field of the monochromatic signal beam, $E_s(x,y)$, can then be obtained.

This method is extended to broadband pulses by spectrally-resolving the reference and signal pulses and generating monochromatic holograms for each frequency in the pulses. If we perform the reconstruction process at different frequencies ω_k (spaced by $\delta\omega$) that satisfy the sampling theorem and cover the bandwidth of the signal and reference pulses, we obtain the electric field $E(x,y)$ for each frequency ω_k. If the spectral phase of the reference pulse is also known, it is straightforward to reconstruct the signal field in the frequency domain, which then yields the complete field in the time domain in the form of an inverse Fourier transform given by the above equation.

To obtain the same information, but on a single camera frame, using STRIPED FISH, we *simultaneously* generate multiple holograms, one for each frequency ω_k. The pulse under test is still interfered with a (coherent and time-coincident) reference pulse at a small vertical angle $\alpha \approx$ 0.5° (about the *x*-axis), but these two pulses then pass through a diffractive optical element (DOE) – equivalent to a low-resolution two-dimensional diffraction grating – which generates a two-dimensional array of replicas of the incident signal and reference pulses, yielding an array of holograms, all with horizontal fringes, where the beams cross (Fig. 27).
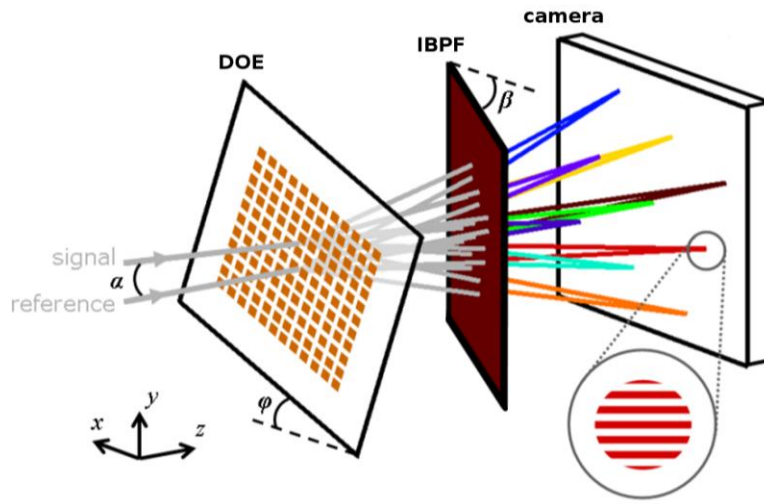

Fig. 27. Three-dimensional view of STRIPED FISH. The signal and reference pulses cross at a small vertical angle α. The DOE is rotated by an angle φ about the *z*-axis, and the IBPF is rotated by an angle β about the *y*-axis. The inset shows one of the spatial interferograms ("digital holograms") captured by the digital camera.

Additionally, a tilted interference band-pass filter (IBPF) spectrally resolves the diffracted beams based on their horizontal propagation angle (Figs. 27 and 28). Finally, we also orient the DOE so that it is rotated slightly by an angle φ about the optical axis *z*. As a result, the hologram array is also slightly rotated, with the effect that each hologram involves pairs of beams of a *different* wavelength. The resulting quasi-monochromatic holograms, each at a different color, yield the complete spatial field (intensity and phase) for each color in the pulse and can then be combined to yield the complete spatio-temporal field of the signal pulse, $E(x,y,t)$.
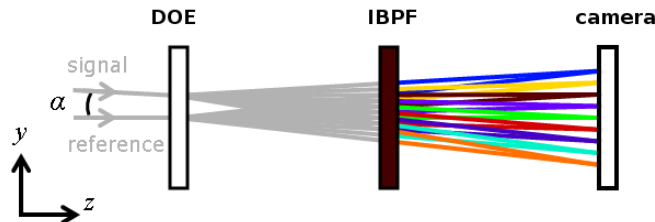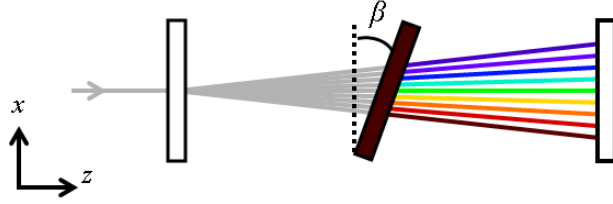
Fig. 28. Top: Side view (*y-z* plane) showing the signal and reference beams crossing at an angle *α*. Bottom: Top view (*x-z* plane) showing how the frequencies transmitted by the IBPF increase with position *x*.

To obtain the complex electric field $E(x,y,\omega)$, we apply a variation of the standard reconstruction algorithm used in many interferometric measurements.[73] Figure 29 depicts the process. First, a two-dimensional Fourier transform is applied to the STRIPED FISH trace. When the different holograms are well separated, the only spatial fringes that are visible are the ones due to the small vertical crossing angle *α* between the signal and the reference pulses. Therefore, in the Fourier domain, we expect to obtain one central region corresponding to the non-interferometric terms, and two other regions corresponding to the interferometric terms due to the crossing angle *α*. We only retain the upper region and inverse-Fourier-transform it to obtain a complex-valued image.

This image contains a collection of spectrally-resolved complex electric fields $E(x,y)$ measured at various frequencies ω_k, once we divide by the field of the reference beam field. These electric fields are distributed over the camera frame and need to be centered one by one. We use data from a reference experimental image obtained from a pulse free of spatio-temporal distortions to find the beam center corresponding to each spatial electric field, so that the data can be reorganized into a three-dimensional data cube, $E(x,y,\omega)$. During this registration step, each digital hologram is assigned a frequency ω_k using calibrated data previously obtained by measuring the spectra of the various diffracted beams.

Finally, we reconstruct the field $E(x,y,t)$ in the time domain. Using diffraction integrals, we can also numerically propagate the electric field through known elements along the *z* direction if desired, to attain the full *four-dimensional* spatio-temporal field, $E(x,y,z,t)$.

As a proof of principle, we set up a STRIPED FISH device as a Mach-Zehnder interferometer (Fig. 30a). A first beam-splitter is used to separate a pre-characterized incident ultrashort pulse from a mode-locked Ti:sapphire oscillator into a reference and a signal pulse. The pulse to be characterized is then sent into the signal arm before the two pulses are recombined on a second beam-splitter. This recombination is quasi-collinear: a small vertical angle *α* is introduced in order to generate horizontal fringes on the digital camera, where both pulses are temporally and spatially overlapped. The temporal overlap is obtained using a delay line that is adjusted to maximize the visibility of the interference fringes.
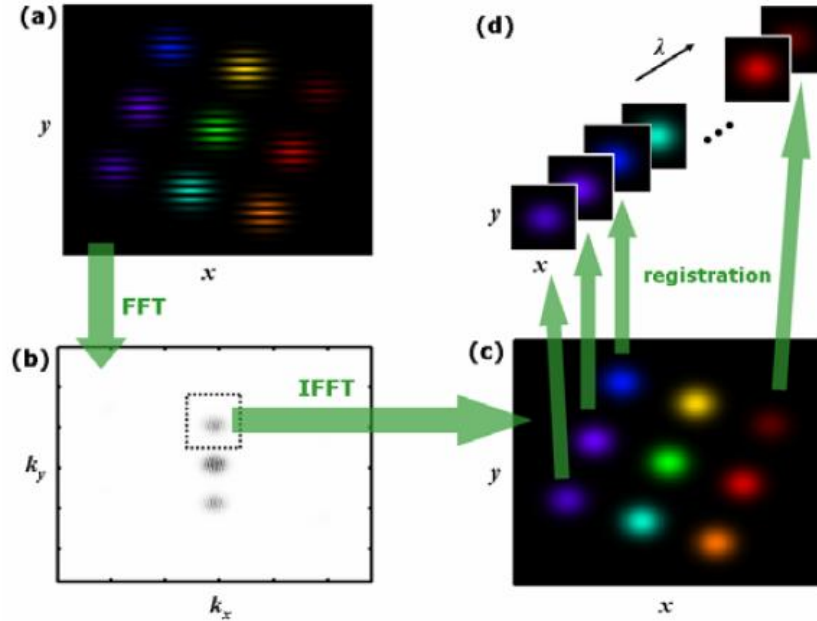
Fig. 29. Algorithm for reconstructing the three-dimensional electric field from a single camera frame. (a) A two-dimensional fast Fourier transform is applied to a simulated STRIPED FISH trace. The interferometric terms are selected in the Fourier plane (b), and transformed back to the original x-y plane (c). The resulting image contains both the spatial amplitude and phase, at the expense of a loss of vertical spatial resolution. (d) A registration step is applied to center all the spatial distributions, and to assign the calibrated wavelengths, in order to obtain the multi-spectral complex data $E(x,y,\omega)$.

Between the second beam-splitter and the digital camera, we insert the rotated DOE and the tilted IBPF to generate the array of spectrally-resolved holograms. The DOE typically consists of an array of 10×10 μm^2 reflective chrome squares, spaced by 50 μm, on the front surface of a quartz substrate. This optic is used in reflection to avoid dispersion from the substrate. Our IBPF has a nominal wavelength $\lambda_n = 837$ nm and a bandwidth of 3 nm, and we tilt it by an angle $\beta \sim 20°$ to transmit the pulses centered at 800 nm. We typically generate an array of a least 20 holograms, which are captured by a high-resolution (5-megapixel) CMOS camera (2208×3000 PixeLINK PL-A781). With this camera, single-shot traces are easily obtained at 800 nm for optical input powers below 100 mW. The wavelength corresponding to each interferogram is calibrated by measuring the local spectrum at that point using a fiber-coupled grating spectrometer.

Figure 30 shows a typical STRIPED FISH trace recorded at Brewster's angle. All the digital holograms can be simultaneously recorded within the dynamic range of a 10-bit digital camera. Note that there is a weak reflection present on the right of the central hologram; it is due to a reflection from the *back* surface of the DOE substrate and could be easily removed by an index-matching element.

We demonstrated STRIPED FISH using ultrashort pulses from a mode-locked Ti:sapphire oscillator. The pulses are centered at 800 nm and have approximately 30 nm of bandwidth (FWHM). Because of the high repetition rate (89 MHz) of the laser, our measurement averages over many pulses. With our 1-kHz chirped-pulse amplified system, recording single-shot STRIPED FISH traces was straightforward, however, since sub-millisecond exposure times are readily obtained by digital cameras.

STRIPED FISH is ideal for measuring spatio-temporal couplings/distortions. As an example, we introduced spatial chirp in the signal beam using a pair of gratings. Figure 31 shows two slices of the reconstructed electric field $E(x,y,t)$ that are obtained by a STRIPED FISH

measurement; one slice is obtained at $y = 0$ (Fig. 31a), and the other at $x = 0$ (Fig. 31b). In these plots, the instantaneous wavelength (shown in color) is calculated from the derivative of the temporal phase. Any temporal gradient of the instantaneous wavelength corresponds to temporal chirp, and any spatial gradient is due to spatial chirp. Horizontal spatial chirp is clearly visible in Fig. 31a.
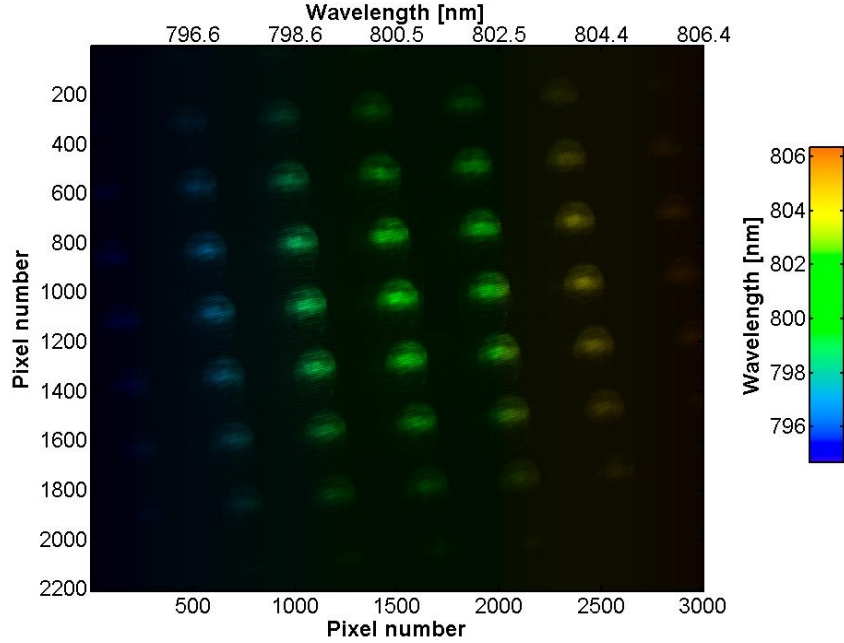

Fig. 30. Experimental STRIPED FISH trace (recorded at Brewster's angle to remove the bright central spot due to the zero-order reflection).
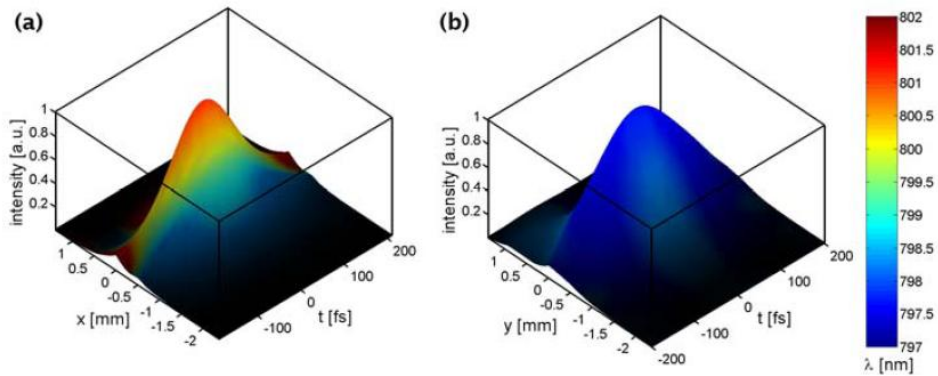

Fig. 31. (a) *x-t* slice of the measured electric field $E(x,y,t)$ of a pulse with spatial chirp. The vertical axis shows the electric field intensity $|E(x,t)|^2$ and the color shows the instantaneous wavelength derived from the phase $\varphi(x,t)$. The spatial gradient of color shows the spatial chirp along the *x* direction. (b) *y-t* slice of the same measured electric field. No spatial chirp is present along the *y* direction, as expected.

With a slight modification, STRIPED FISH can be fully self-referenced, so the device requires only one input pulse, the pulse under test. This pulse is split into two replicas, one of which is spatially filtered to yield a reference pulse (a pulse whose *spatial* phase is essentially

37

constant). The *spectral* phase of that reference pulse is therefore free of any spatial dependence, and is measured by a FROG device (in our case, a Swamp Optics GRENOUILLE) matched to the pulse characteristics. This completely characterizes the reference pulse that can then be interfered with the signal pulse in the usual configuration.

Finally, we note that it is possible to quantify the overall performance of STRIPED FISH with regard to the spatio-temporal complexity it can support. Indeed, the maximum *time*-bandwidth product (TBP) that we can hope to measure is roughly equal to the number of holograms that are captured. Similarly, the maximum *space*-bandwidth product (SBP) is approximately equal to the number of spatial points obtained by the reconstruction algorithm. As a result, the amount of information (number of independent data points), and therefore the maximum pulse complexity that STRIPED FISH can measure is estimated by introducing the *space-time-bandwidth product* TBP×SBP, which is usually on the order of 10^5, about one hundredth to one tenth the number of camera pixels.

Wavelength-multiplexed digital holography allows us for the first time to completely characterize (i.e., in intensity and phase and as a function of three dimensions x, y and t) the electric field of a femtosecond laser pulse using a configuration compatible with single-shot detection. We experimentally implemented it using a simple device (STRIPED FISH) based on only a few key elements: a diffractive beam splitter, a spectral filter and a high-resolution digital camera.

Outlook

It is now possible to measure almost every characteristic of almost every ultrashort pulse. And the techniques for doing so are relatively simple. While, as always, many unsolved measurement problems remain, including single-shot measurement of the complete spatio-temporal field of a single focused pulse and the measurement of the complete spatio-temporal field of extremely complex or intense pulses, such as filaments or continuum generated in bulk (we tried using STRIPED FISH to do this latter measurement; however, the continuum proved too complex in space). But these unsolved problems are becoming ever more obscure. What remains now is to use these methods to learn more about these ephemeral events and the many applications for which they are used.

Acknowledgments

References

1. J.A. Giordmaine, P.M. Rentzepis, S.L. Shapieo, and K.W. Wecht, *Two-Photon Excitation of Fluorescence by Picosecond Light Pulses.* Appl. Phys. Lett., 1967. **11**(7): p. 216-218.
2. R. Trebino, *Frequency-Resolved Optical Gating: The Measurement of Ultrashort Laser Pulses.* 2002, Boston: Kluwer Academic Publishers.
3. H. Stark, ed. *Image Recovery: Theory and Application*. 1987, Academic Press: Orlando.
4. E.J. Akutowicz, *On the Determination of the Phase of a Fourier Integral, I.* Trans. Amer. Math. Soc., 1956. **83**(September): p. 179-192.
5. E.J. Akutowicz, *On the Determination of the Phase of a Fourier Integral, II.* Trans. Amer. Math. Soc., 1957. **84**: p. 234-238.
6. R. Trebino, E.K. Gustafson, and A.E. Siegman, *Fourth-Order Partial-Coherence Effects in the Formation of Integrated-Intensity Gratings with Pulsed Light Sources.* J. Opt. Soc. Amer. B, 1986. **3**: p. 1295.
7. J.C. Diels, J.J. Fontaine, I.C. McMichael, and F. Simoni, *Control and Measurement of Ultrashort Pulse Shapes (in Amplitude and Phase) with Femtosecond Accuracy.* Appl. Opt., 1985. **24**(9): p. 1270-1282.
8. C. Yan and J.C. Diels, *Amplitude and Phase Recording of Ultrashort Pulses.* J. Opt. Soc. of Amer. B, 1991. **8**(6): p. 1259-1263.
9. J.C. Diels and J.J. Fontaine, *Coherence Properties of Ultrashort Optical Pulses.* J. Opt. (Paris), 1985. **16**(3): p. 115-119.
10. J.C.M. Diels, J.J. Fontaine, N. Jamasbi, and M. Lai. *The Femto-nitpicker*. in *Conference on Lasers & Electro-Optics*. 1987.
11. J.-H. Chung and A.M. Weiner, *Ambiguity of ultrashort pulse shapes retrieved from the intensity autocorrelation and power spectrum.* IEEE J. Sel. Top. Quant. Electron., 2001. **7**(4): p. 656-666.
12. D.J. Kane and R. Trebino, *Single-Shot Measurement of the Intensity and Phase of an Arbitrary Ultrashort Pulse By Using Frequency-Resolved Optical Gating.* Opt. Lett., 1993. **18**(10): p. 823-825.
13. D.J. Kane and R. Trebino, *Characterization of Arbitrary Femtosecond Pulses Using Frequency Resolved Optical Gating.* IEEE J. of Quant. Electron., 1993. **29**(2): p. 571-579.
14. R. Trebino and D.J. Kane, *Using Phase Retrieval to Measure the Intensity and Phase of Ultrashort Pulses: Frequency-Resolved Optical Gating.* J. Opt. Soc. Amer. A, 1993. **10**(5): p. 1101-1111.
15. E. Zeek, A.P. Shreenath, M. Kimmel, and R. Trebino, *Simultaneous Automatic Calibration and Direction-of-Time-Ambiguity Removal in Frequency-Resolved Optical Gating.* Appl. Phys. B, 2002. **B74**: p. S265-271.
16. B. Yellampalle, K.Y. Kim, and A.J. Taylor, *Amplitude ambiguities in second-harmonic-generation frequency-resolved optical gating.* Opt. Lett., 2007. **32**(24): p. 3558-3561.
17. L. Xu, D.J. Kane, and R. Trebino, *Comment on "Amplitude ambiguities in second-harmonic generation frequency-resolved optical gating" by B. Yellampalle, K.Y. Kim, and A. J. Taylor.* Opt. Lett., submitted, 2008.
18. Y. Mairesse and F. Quéré, *Frequency-resolved optical gating for complete reconstruction of attosecond bursts.* Phys Rev A, 2005. **71**: p. 011401.
19. G. Sansone, E. Benedetti, C. Vozzi, S. Stagira, and M. Nisoli, *Attosecond metrology in the few-optical-cycle regime.* New J. Phys., 2008. **10**: p. 025006.
20. J.R. Birge, R. Ell, and F.X. Kärtner, *Two-dimensional spectral shearing interferometry for few-cycle pulse characterization.* Opt. Lett., 2006. **31**(13): p. 2063-2065.
21. P. Gabolde and R. Trebino, *Single-shot measurement of the full spatiotemporal field of ultrashort pulses with multispectral digital holography.* Opt. Expr., 2006. **14**(23): p. 11460.
22. P. Gabolde and R. Trebino, *Single-frame measurement of the complete spatio-temporal intensity and phase of ultrashort laser pulse(s) using wavelength-multiplexed digital holography.* J. Opt. Soc. Am. B, 2008. **25**(6): p. A25-A33.
23. P. Bowlan, P. Gabolde, A. Shreenath, K. McGresham, R. Trebino, and S. Akturk, *Crossed-beam spectral interferometry: a simple, high-spectral-resolution method for completely characterizing complex ultrashort pulses in real time.* Opt. Expr., 2006. **14**(24): p. 11892.
24. P. Bowlan, P. Gabolde, and R. Trebino, *Directly measuring the spatio-temporal electric field of focusing ultrashort pulses.* Opt. Expr., 2007. **15**: p. 10219-10230.
25. P. Bowlan, P. Gabolde, M.A. Coughlan, R. Trebino, and R.J. Levis, *Measuring the spatio-temporal electric field of ultrashort pulses with high spatial and spectral resolution.* J. Opt. Soc. Am. B, 2008. **25**(6): p. A81-A92.
26. P. O'Shea, S. Akturk, M. Kimmel, and R. Trebino, *Practical Issues in the Measurement of Ultrashort Pulses Using GRENOUILLE.* Appl. Phys. B, 2004. **79**(6): p. 683 - 691.

27. P. O'Shea, M. Kimmel, X. Gu, and R. Trebino, *Highly simplified device for ultrashort-pulse measurement.* Opt. Lett., 2001. **26**(12): p. 932-934.

28. C. Radzewicz, P. Wasylczyk, and J.S. Krasinski, *A poor man's FROG.* Opt. Commun., 2000. **186**(4-6): p. 329-333.

29. S. Akturk, M. Kimmel, P. O'Shea, and R. Trebino, *Measuring pulse-front tilt in ultrashort pulses using GRENOUILLE.* Opt. Expr., 2003. **11**(5): p. 491-501.

30. S. Akturk, M. Kimmel, P. O'Shea, and R. Trebino, *Measuring spatial chirp in ultrashort pulses using single-shot Frequency-Resolved Optical Gating.* Opt. Expr., 2003. **11**(1): p. 68-78.

31. L. Xu, E. Zeek, and R. Trebino, *Simulations of Frequency-Resolved Optical Gating for measuring very complex pulses.* J. Opt. Soc. Am. B, 2008. **25**(6): p. A70-A80.

32. J.K. Ranka, R.S. Windeler, and A.J. Stentz, *Visible continuum generation in air-silica microstructure optical fibers with anomalous dispersion at 800 nm.* Opt. Lett., 1999. **25**(1): p. 25-27.

33. X. Gu, L. Xu, M. Kimmel, E. Zeek, P. O'Shea, A.P. Shreenath, R. Trebino, and R.S. Windeler, *Frequency-resolved optical gating and single-shot spectral measurements reveal fine structure in microstructure-fiber continuum.* Opt. Lett., 2002. **27**(13): p. 1174-1176.

34. A.L. Gaeta, *Nonlinear propagation and continuum generation in microstructured optical fibers.* Opt. Lett., 2002. **27**(11): p. 924-926.

35. M.A. Foster, A.L. Gaeta, Q. Cao, and R. Trebino, *Soliton-effect compression of supercontinuum to few-cycle durations in photonic nanowires.* Opt. Expr., 2005. **13**(18): p. 6848-6855.

36. M.A. Foster, J.M. Dudley, B. Kibler, Q. Cao, D. Lee, R. Trebino, and A.L. Gaeta, *Nonlinear pulse propagation and supercontinuum generation in photonic nanowires: experiment and simulation.* Appl. Phys. B, 2005. **B81**(2-3): p. 363-367.

37. J. Dudley, X. Gu, X. Lin, M. Kimmel, E. Zeek, P. O'Shea, R. Trebino, S. Coen, and R.S. Windeler, *Cross-correlation frequency resolved optical gating analysis of broadband continuum generation in photonic crystal fiber: simulations and experiments.* Opt. Expr., 2002. **10**(21): p. 1215-1221.

38. Q. Cao, X. Gu, E. Zeek, M. Kimmel, R. Trebino, J. Dudley, and R.S. Windeler, *Measurement of the intensity and phase of supercontinuum from an 8-mm-long microstructure fiber.* Appl. Phys. B, 2003. **77**: p. 239-244.

39. S. Haacke, S. Schenkl, S. Vinzani, and M. Chergui, *Femtosecond and Picosecond Fluorescence of Native Bacteriorhodopsin and a Nonisomerizing Analog.* Biopolymers, 2002: p. 306-309.

40. J. Zhang, A.P. Shreenath, M. Kimmel, E. Zeek, R. Trebino, and S. Link, *Measuring of the intensity and phase of attojoule femtosecond light pulses using optical-parametric-amplification cross-correlation frequency-resolved optical gating.* Opt. Expr., 2003. **11**(6): p. 601-609.

41. S. Akturk, M. Kimmel, P. O'Shea, and R. Trebino, *Extremely simple device for measuring 20-fs pulses.* Opt. Lett., 2004. **29**(9): p. 1025-1027.

42. R. Levis, Gerahun Menkir, Herschel Rabitz, *Selective Bond Dissociation and Rearrangement with Optimally Tailored, Strong-Field Laser Pulse.* Science, 2001. **292**(5517): p. 709.

43. A. Assion, T. Baumert, M. Bergt, T. Brixner, B. Kiefer, V. Seyfried, M. Strehle, and G. Gerber, *Control of Chemical Reactions by Feedback-Optimized Phase-Shaped Femtosecond Laser Pulses.* Science, 1998. **282**: p. 919-922.

44. N. Dudovich, D. Oron, and Y. Silberberg, *Single-pulse coherently controlled nonlinear Raman spectroscopy and microscopy.* Nature, 2002. **418**: p. 512-514.

45. D. Meshulach and Y. Silberberg, *Coherent quantum control of two-photon transitions by a femtosecond laser pulse.* Nature, 1998. **396**(6708): p. 239-242.

46. D.N. Fittinghoff, J.L. Bowie, J.N. Sweetser, R.T. Jennings, M.A. Krumbügel, K.W. DeLong, R. Trebino, and I.A. Walmsley, *Measurement of the Intensity and Phase of Ultraweak, Ultrashort Laser Pulse.* Opt. Lett., 1996. **21**(12): p. 884-886.

47. J.P. Geindre, P. Audebert, S. Rebibo, and J.C. Gauthier, *Single-shot spectral interferometry with chirped pulses.* Opt. Lett., 2001. **26**(20): p. 1612-1614.

48. K. Misawa and T. Kobayashi, *Femtosecond Sangac interferometer for phase spectroscopy.* Opt. Lett., 1995. **20**(14).

49. A.C. Kovaecs, K. Osvay, Bor, Zs, *Group-delay measurement on laser mirrors by spectrally resolved white-light interferometry.* Opt. Lett., 1995. **20**(7): p. 788-791.

50. A.P. Kovaecs, K. Osvay, G. Kurdi, M. Gorbe, J. Klenbniczki, and Z. Bor, *Dispersion Control of a pulse stretcher-compressor system with two-dimensional spectral interferometry.* Appl. Phys. B, 2005. **80**: p. 165-170.

51. D. Meshulach, D. Yelin, and Y. Silbergerg, *Real-Time Spatial-Spectral Interference Measureents of Ultrashort Optical Pulses.* J. Opt. Soc. Am. B, 1997. **14**(8): p. 2095-2098.

52. E.M. Kosik, A.S. Radunsky, I. Wamsley, and C. Dorrer, *Interferometric technique for measuring broadband ultrashort pulses at the sampling limit.* Opt. Lett., 2005. **30** (3): p. 326-328.
53. J.J. Field, T.A. Planchon, W. Amir, C.G. Durfee, and J.A. Squier, *Characterization of a high efficiency, ultrashort pulse shaper incorporating a reflective 4096-element spatial light modulator.* Opt. Commun., 2007. **287**: p. 368-376.
54. R. Trebino, P. O'Shea, M. Kimmel, and X. Gu, *Measuring Ultrashort Laser Pulses Just Got a Lot Simpler.* Optics & Photonics News, 2001. **12**(6): p. 22-25.
55. M. Kempe and W. Rudolph, *Impact of chromatic and spherical aberration on the focusing of ultrashort light pulses by lenses.* Opt. Lett., 1993. **18**: p. 137-139.
56. M. Kempe and W. Rudolph, *Femtosecond pulses in the focal region of lenses.* Phys. Rev. A, 1993. **48**(6): p. 4721-4729.
57. Z. Bor, *Distortion of femtosecond laser pulses in lenses.* Opt. Lett., 1989. **14**(2): p. 119-121.
58. U. Fuchs, U.D. Zeitner, and A. Tuennermann, *Ultra-short pulse propagation in complex optical systems.* Opt. Expr., 2005. **13**(10): p. 9903-9908.
59. V.V. Lozovoy, I. Pastirk, and M. Dantus, *Multiphoton intrepulse interference. IV. Ultrashort pulse spectral phase characterization and compensation.* Opt. Lett., 2004. **29**(7): p. 775-777.
60. D.N. Fittinghoff, J.A. Squier, C.P.T. Barty, J.N. Sweetser, R. Trebino, and M. Muller, *Collinear type II second-harmonic-generation frequency-resolved optical gating for use with high-numerical-aperture objectives.* Opt. Lett., 1998. **23**(13): p. 1046-1048.
61. R. Chadwick, E. Spahr, J.A. Squier, and C.G. Durfee, *Fringe-free, background-free, collinear third-harmonic generation frequency-resolved optical gating measurements for multiphoton microscopy.* Opt. Lett., 2006. **31**(22): p. 3366-3368.
62. W. Amir, T.A. Planchon, C.G. Durfee, J.A. Squier, P. Gabolde, R. Trebino, and M. Mueller, *Simultaneous visualizations of spatial and chromatic aberrations by two-dimensional Fourier transform spectral interferometry.* Opt. Lett., 2006. **31**(19): p. 2927-2929.
63. S. Akturk, X. Gu, P. Gabolde, and R. Trebino, *The general theory of first-order spatio-temporal distortions of Gaussian pulses and beams.* Opt. Expr., 2005. **13**: p. 8642-8661.
64. S. Akturk, X. Gu, E. Zeek, and R. Trebino, *Pulse-front tilt caused by spatial and temporal chirp.* Opt. Expr., 2004. **12**(19): p. 4399-4410.
65. Z. Bor and Z.L. Horvath, *Distortion of femtosecond pulses in lenses. Wave optical description.* Opt. Commun., 1992. **94**(4): p. 249-258.
66. Z. Bor, B. Racz, G. Szabo, M. Hilbert, and H.A. Hazim, *Femtosecond pulse front tilt caused by angular dispersion.* Opt Eng, 1993. **32**(10): p. 2501-2504.
67. M. Kempe and W. Rudolph, *Impact of chromatic and spherical aberration on the focusing of ultrashort light pulses by lenses.* Opt. Lett., 1993. **18**(2): p. 137-139.
68. J. Néauport, N. Blanchot, C. Rouyer, and C. Sauteret, *Chromatism compensation of the PETAL multipetawatt high-energy laser.* Appl. Opt., 2007. **46**(9): p. 1568-1574.
69. G. Pretzler, A. Kasper, and K.J. Witte, *Angular chirp and tilted light pulses in CPA lasers.* Appl. Phys. B, 2000. **70**: p. 1-9.
70. T. Tanabe, H. Tanabe, Y. Teramura, and F. Kannari, *Spatiotemporal measurements based on spatial spectral interferometry for ultrashort optical pulses shaped by a Fourier pulse shaper.* J. Opt. Soc. Am. B, 2002. **19**(11): p. 2795-2802.
71. K. Varju, A.P. Kovacs, G. Kurdi, and K. Osvay, *High-precision measurement of angular dispersion in a CPA laser.* Appl. Phys. B, 2002. **Suppl.**: p. 259-263.
72. P. Gabolde and R. Trebino, *Self-referenced measurement of the complete electric field of ultrashort pulses.* Opt. Expr., 2004. **12**(19): p. 4423 - 4429.
73. M. Takeda, H. Ina, and S. Kobayashi, *Fourier-transform method of fringe-pattern analysis for computer-based topography and interferometry.* J. Opt. Soc. Am., 1982. **72**(1): p. 156-160.
74. R. Trebino, K.W. DeLong, D.N. Fittinghoff, J.N. Sweetser, M.A. Krumbuegel, and D.J. Kane, *Measuring Ultrashort Laser Pulses in the Time-Frequency Domain Using Frequency-Resolved Optical Gating.* Rev. Sci. Instrum., 1997. **38**: p. 3277-3295.
75. Z. Liu, M. Centurion, G. Panotopoulos, J. Hong, and D. Psaltis, *Holographic recording of fast events on a CCD camera.* Opt. Lett., 2002. **27**(1): p. 22-24.
76. S. Grilli, P. Ferraro, S. De Nicola, A. Finizo, G. Pierattini, and R. Meucci, *Whole optical wavefield reconstruction by Digital Holography.* Opt. Express, 2001. **9**(6): p. 294-302.